

*A System for Measurement of Photosynthesis in the Aerial Portion of a Plant*

Engineering 90 Senior Design Project

Marie Cosgrove-Davies and Lauren Goodfriend  
Advised by Professor McGarity and Professor Machado (Biology)

8<sup>th</sup> May 2008

## **Acknowledgments**

Many thanks to our advisors, Professor McGarity and Professor Machado, for giving us excellent advice; Ed Jaoudi, for buying electronic equipment for us and never getting frustrated; Grant “Smitty” Smith, Doug Judy, Don Reynolds, and Steve Palmer, for helping with chamber construction; Holly Castleman, for just being generally awesome; and Anson Stewart, Carl Shapiro, and Travis Rothbloom, for running E14 tests of the properties of our dessicant.

## Table of Contents

Introduction.....	4
The LI-6400: An Overview .....	7
Theory and Design.....	8
Calculation of Photosynthesis.....	8
Measurement Chamber Design.....	9
Humidity Control.....	12
Desiccant Column.....	12
Humidifying Column.....	14
Sizing of Temperature Controls.....	17
Fluid Flow Analysis.....	19
Valve Sizing.....	21
Boundary Layer Calculations .....	24
Mixing.....	25
Electrical Signal Calculations.....	25
System Construction.....	27
Sample Collection Subsystem Construction.....	28
Humidity Control System Construction.....	29
Humidity Control Columns.....	29
Connections in the Humidity Control System .....	31
Inlet Measurement System Construction.....	32
Measurement Chamber Construction .....	33
Temperature Control Unit Construction.....	34
Critical Components of Control and Measurement System .....	37
Blower.....	37
Control valves.....	37
Mass flow meter.....	38
Sampling pump.....	38
Electrical Components.....	39
Programming on the LI-6400.....	39
Testing.....	40
Blower Compatibility Problems .....	40
Calibration of Volumetric Flow Meter .....	41
System Curve Test.....	42
Chamber Mixing Test.....	44
Light Loss Tests.....	46
Temperature Control System Tests.....	47
Gas Exchange Test.....	51
Volumetric Leak Test .....	55
Humidity Control Column Test.....	55
Future Work.....	57
References.....	59

## Introduction

The objective in this project was to convert the LI-6400 infrared photosynthesis measurement system from its default state of observing a small portion of a leaf to allow the device to observe photosynthesis in an entire plant. In order to accomplish this, a plant containment chamber was designed, built, and instrumented; and the LI-6400's settings were adapted to allow it to interact with and measure from the chamber.

Photosynthesis is the conversion of light into chemical energy by plants. It requires water and carbon dioxide and produces oxygen and carbohydrates. The basic photosynthesis equation is  $6CO_2 + 6H_2O + sunlight \rightarrow C_6H_{12}O_6 + 6O_2$ . Photosynthesis depends on a number of environmental factors including light, carbon dioxide levels, humidity, wind speed, and temperature. As the energy input to the reaction, light levels have a direct effect on photosynthetic rates. Photosynthetic rates increase with light until a saturation point is reached. This effect is currently well-understood. As reagents, carbon dioxide and water vapor have an obvious effect on photosynthesis. In addition, ambient relative humidity controls the opening of the stomata, through which gas exchange to the plant occurs. At extremely high or low humidity levels, the stomata will close, limiting photosynthesis. Wind speed governs the thickness of the boundary layer to the leaf. Thicker boundary layers result in slower diffusion of gases into the leaf. Temperature mainly affects the performance of enzymes that help catalyze photosynthetic reactions.

In 1727, Stephan Hales was the first recorded person to suggest that some of plants' energy might be derived from light. In 1772 Joseph Priestly found that plants gave off a gas that allowed a candle to continue burning in a closed chamber, and when informed of these results in 1783, French chemist Antoin-Laurent Lavoiser saw the theoretical

implications and named the gas oxygen. Chlorophyll was isolated in 1817 by Pelletier and Caventou, and in 1845 Robert Mayer put forth the theory that plants transform the energy of the sun into chemical energy. It was in 1862 that the overall photosynthesis equation was produced. Study of photosynthesis continued to progress. In the mid 20<sup>th</sup> century, a number of new techniques were developed that allowed for more precise examination of the phenomenon. These techniques include climatized growth chambers, electron microscopy, and fluorescence spectrophotometry. Research into photosynthesis continues to this day. In 1983 LI-Cor introduced its first gas exchange system, the LI-6000.

The LI-6400 (Figure 1) is LI-Cor's third generation gas exchange system. It uses a sensor head containing an infrared gas analysis (IRGA) to measure photosynthesis (Figure 2). In its default configuration, the sensor head clamps down on a small cross-section of a leaf, the console specifies the leaf air conditions, and the results are monitored. The data from the small sample can then be generalized by scaling up, assuming that the photosynthesis per unit area of the leaf is the same as the photosynthesis per area of the entire plant. This assumption has some clear problems: different leaves may receive different amounts of sunlight; older and younger leaves might photosynthesize differently; estimation of area is approximate. There are numerous objections which could be raised as regards the accuracy of this method.

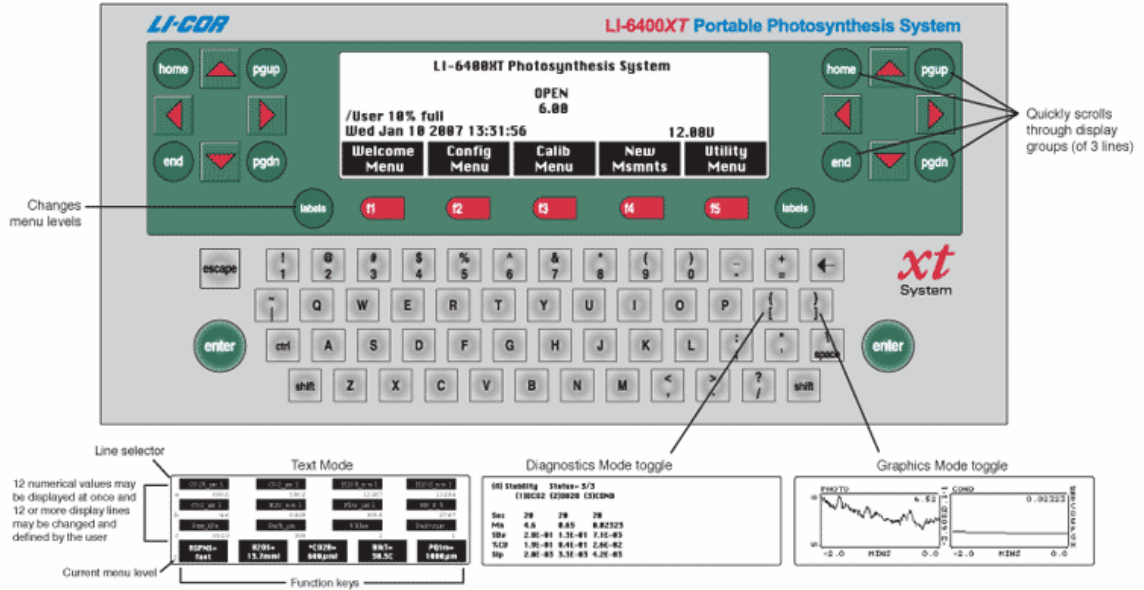


**Figure 1. LI-6400 console (from [www.licor.com](http://www.licor.com))**

As a way of resolving these objections, it was determined that a chamber capable of containing an entire plant would be a reasonable solution. The chamber should allow for control of carbon dioxide and humidity levels in the incoming air, and should be temperature controlled as well as allowing for free circulation of air. Using such a chamber, the actual photosynthesis of the entire plant could be measured, rather than estimated from the photosynthesis of a small portion of a leaf.

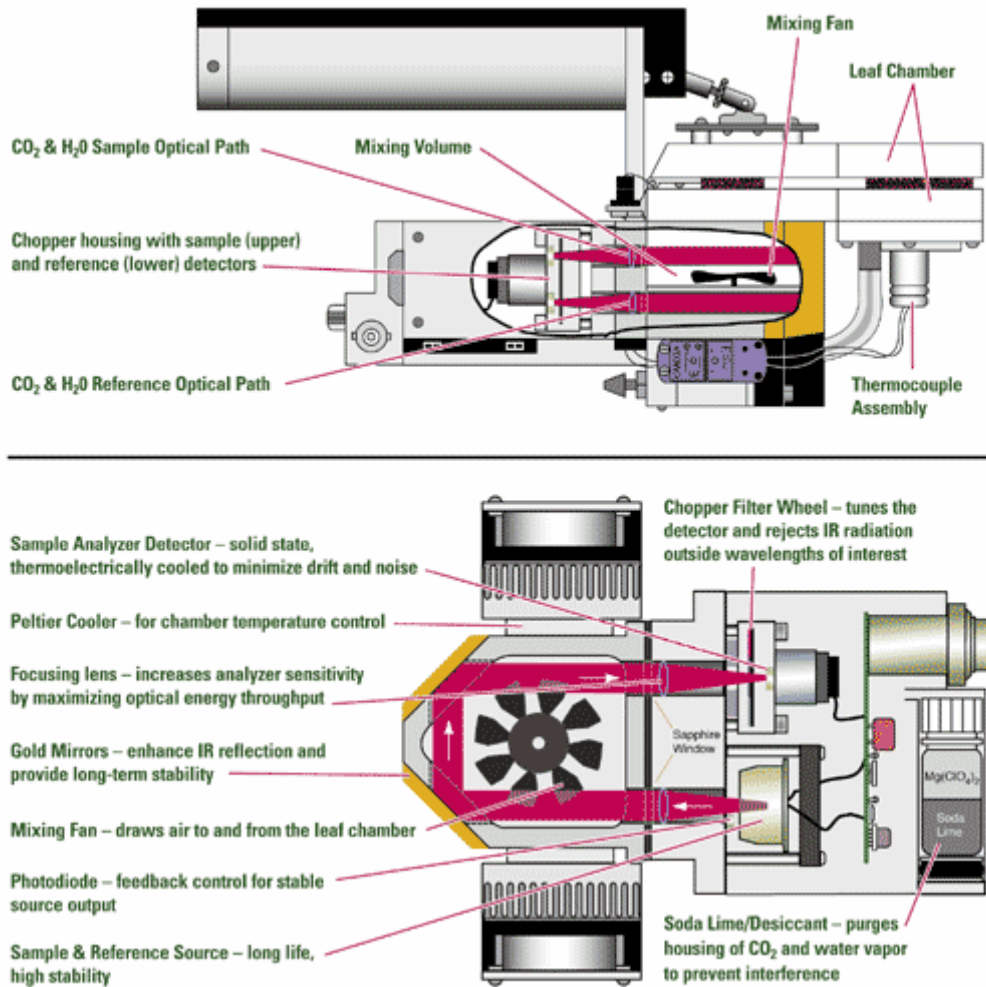


**Figure 2. LI-6400 sensor head (from [www.licor.com](http://www.licor.com))**

*The LI-6400: An Overview*

The LI-6400 is an open system, meaning that the differences in water and carbon dioxide concentrations between the incoming and outgoing air are measured and used to calculate photosynthesis. In a closed system, no air exits or enters the environment, allowing the environment to come to a steady state. By contrast, open systems allow air to enter and exit, measuring both intake and outtake flows in order to determine the effects of the system being tested (here, a plant). Open systems allow for conditioning of

incoming air, which makes it possible to standardize humidity, carbon dioxide concentration, temperature, and other important parameters.

In its normal configuration, the LI-6400 sensor head clamps on to a small portion of a leaf as described above. The cuvette contained within the sensor head is where all measurements take place. For speed of measurement and convenience, the LI-6400's IRGAs are in the sensor head rather than in the console, which would cause a lag in measurements.

The LI-6400 is able to condition the air going into the cuvette by filtering it or adding gas, and it can control the chamber conditions using built-in Peltier units and a small light source. By controlling these variables, it can obtain response curves of the plant to light, CO<sub>2</sub> concentration, temperature, and humidity.

The console or "brain" portion of the LI-6400 is connected to the sensor head by tubes for air and cables for data. It contains 128 Mbytes of dynamic memory, 64 Mbytes of flash memory, a 200 MHz, 32 bit processor, and runs on an underlying operating system of LINUX. In the factory configuration, the console treats the air that goes into the sensor head and disposes of air returning from the sensor head. It also processes and records measurements taken. Data can be displayed as a number or in a chart. The console supports a low-level programming language called LPL and a high-level operating system called OPEN, which is a subset of the LPL language with many pre-defined parameters, functions, and programs.

## **Theory and Design**

### *Calculation of Photosynthesis*

The LI-4600 uses the following equations to determine photosynthesis.

To measure transpiration, the mass balance of water vapor in an open system must first be written. This equation is  $sE = u_o w_o - u_i w_i$ , where  $s$  is the leaf area ( $\text{m}^2$ ),  $E$  is the transpiration rate ( $\text{mol m}^{-2} \text{s}^{-1}$ ),  $u_i$  and  $u_o$  are incoming and outgoing flow rates ( $\text{mol s}^{-1}$ ), and  $w_i$  and  $w_o$  are incoming and outgoing water mole fractions ( $\text{mol H}_2\text{O mol air}^{-1}$ ). Because transpiration causes the exit flow rate to be greater than the incoming flow rate, the two terms cannot be collapsed easily. Using the simplification  $u_o = u_i + sE$ , the

$$\text{equation becomes } E = \frac{u_i(w_o - w_i)}{s(1 - w_o)}.$$

The variable  $w_l$  ( $\text{mmol H}_2\text{O (mol air)}^{-1}$ ), the molar concentration of water vapor within the plant, is measured using leaf temperature  $T_l$  (C) and atmospheric pressure  $P$

(kPa) using the equation  $W_l = \frac{e(T_l)}{P} \times 1000$ . Here, the function  $e(T)$  is the saturation

vapor pressure at temperature  $T$ . The formula used is  $e(T) = 0.61365e^{\frac{17.502T}{240.97+T}}$ . Using this value for  $W_l$ , the total conductance to water vapor can be measured:

$$g_{tw} = \frac{E \left( 1000 - \frac{W_l + W_s}{2} \right)}{W_l - W_s}.$$

The net photosynthesis of the plant is calculated using the equation

$sa = u_i c_i - u_o c_o$ . Here,  $a$  is the assimilation rate ( $\text{mol CO}_2 \text{ m}^{-2} \text{ s}^{-1}$ ) and  $c_i$  and  $c_o$  are incoming and outgoing mole fractions of carbon dioxide ( $\text{mol CO}_2 \text{ mol air}^{-1}$ ). By the

relationship above, this equation can be rewritten as  $a = \frac{u_i(c_i - c_o)}{s} - Ec_o$  to find  $a$ .

### Measurement Chamber Design

The dimensions of the measurement chamber are 8" x 8" x 10" (Figure 3). These dimensions were chosen in consultation with Prof. Machado to best contain the tropical

seedlings he intends to study. The measurement chamber attaches to the base on a 4" lip. The lip dimension was chosen as a compromise between ease of transport and reducing gas exchange, as well as chamber stability. A layer of rubber between the chamber and the base reduces gas exchange through this interface. The base consists of two halves with a rubber-lined lap joint between them. A slot at the center of the joint in both halves allows the base to be closed around a plant stem, and the resulting hole for the plant stem is 1/2" in diameter. This diameter was chosen using data collected by Prof. Machado (Figure 4).

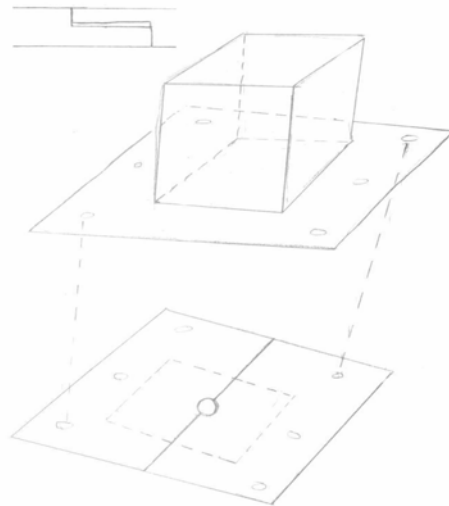


**Figure 3. Initial chamber design**

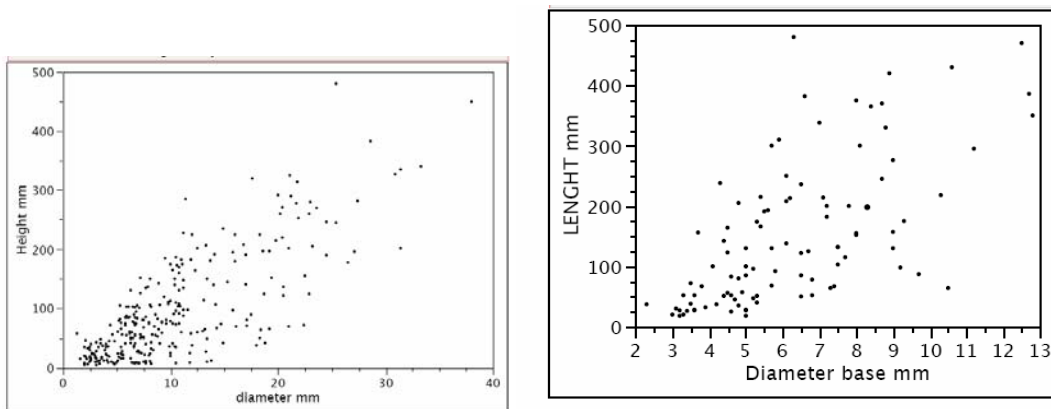


**Figure 4. Plant height and length vs. stem diameter**

The measurement chamber was designed in clear acrylic sheet, trade name Plexiglas. This material is both optically clear (transmissivity in visible spectra is generally greater than 90%) and light (density is  $1180 \text{ kg/m}^3$ ) ([http://www.boedeker.com/acryl\\_p.htm](http://www.boedeker.com/acryl_p.htm)). Acrylic has some non-optimal qualities, namely that it is somewhat brittle and permeable to carbon dioxide. The primary alternative material considered was glass, which is much heavier ( $5000 \text{ kg/m}^3$ ) and also fragile, but impermeable to gases. Since this system is intended to be portable, acrylic was chosen. Clear Teflon tape lining on the inside of the chamber was used to reduce gas exchange through the walls of the chamber.

The chamber walls were designed with intended compass direction orientation. The south wall of the chamber is unobstructed to allow maximum light infiltration. The north wall is covered to a large extent by the temperature control unit and also contains three sealing glands. The sealing glands allow wires to pass out of the chamber without incurring gas exchange. Unlike using caulk, the glands are reusable so wires can be repeatedly removed and reinserted. Three sealing glands were used: two 5 mm glands for the fans, humidity sensor, thermocouple, and quantum sensor and one 15 mm gland for the wires going to the thermoelectric coolers. The east and west walls contain the inlet and outlet respectively as well as two mixing fans. The mixing fan placement was chosen to maximize air circulation by providing mixing energy on both sides of the chamber and at two levels while avoiding directing air directly at the input or output. By placing the mixing fans above and below the inlet and outlet, their outflow works with the inlet and outlet to mix air.

## Humidity Control

### *Desiccant Column*

Due to the range of input relative humidities, silica gel was chosen as the desiccant. Other desiccants, such as activated alumina and molecular sieves, only perform well within specific humidity ranges. Although silica gel also adsorbs carbon dioxide, it only adsorbs 2% of its weight, compared with up to 40% of its weight in water vapor. Since carbon dioxide concentration was not actively controlled for, this effect was considered acceptable.

The volume of silica gel required for continuous 24 hour operation of the measurement chamber was determined under a conservative scenario. At a flow rate of 11 gpm, saturated air at 27 C entered the system and required dehumidification to 30% relative humidity. This reduction in relative humidity at the given flow rate corresponds to a removal of 1.1 kg/day of water vapor. Silica gel can adsorb 33% of its weight in water at 70% relative humidity, leading to a need for 3.3 kg/day of silica gel, or about 4.6 L/day including voids (Figure 5). Since the system is intended for measuring photosynthesis rather than general gas exchange, the system was sized to adsorb half that amount, or only during the half of the day with the most solar radiation. The volume and mass of silica gel needed to operate under the conservative scenario for 24 hours was also considered excessively large. Thus, the system instead is designed to hold 1.7 kg of silica gel, or 2.3 liters, for 12 hours of continuous operation. Unless gas exchange measurements are made at night, this mass of silica gel should be sufficient.

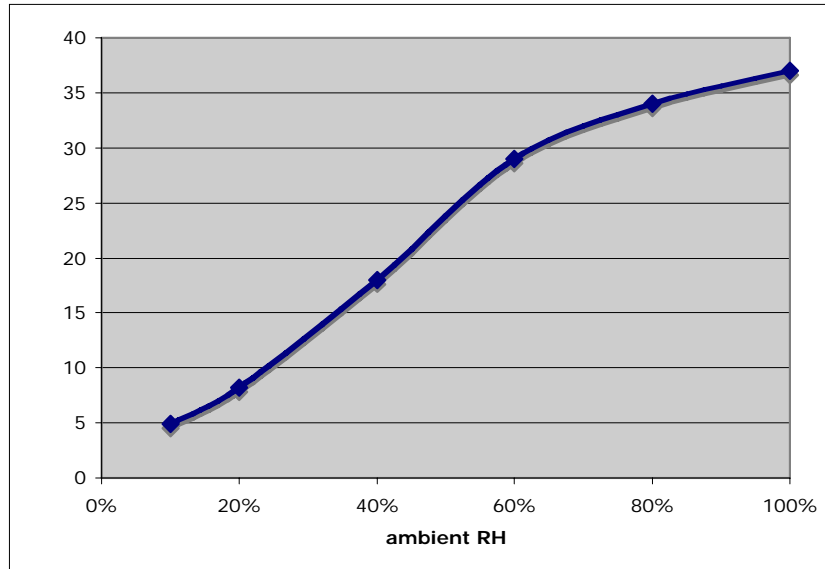


**Figure 5. Silica gel absorption capacity**

(Data from <http://www.ecompressedair.com/desiccant/silicagel.shtml>)

The silica gel purchased was grade 22, spherical silica gel granules of 2 – 5 mm diameter. This grade is made particularly for dehumidifying dynamic gas streams.

Properties given by the manufacturer are listed in Table 1.

Diameter	2 - 5	mm
Surface area	760	m <sup>2</sup> /g
Pore volume	0.43	cm <sup>3</sup> /g
Porosity	0.3096	
Bulk density	0.72	kg/L

**Table 1. Properties of silica gel**

The sizing of the dehumidifying column was based on the LUB-equilibrium method of packed beds. This method uses the concept of the stoichiometric length, the length of the packed bed that is at equilibrium with the influent concentration. The stoichiometric length at a specified breakthrough time is the minimum length of the packed bed. This quantity is given by

$$L_s = \frac{u_s(C_{A0} - C_{A,init})t_b M_A}{\rho(q_A^\infty - q_{A0})}$$

where  $u_s$  is the superficial velocity,  $C_{A0}$  and  $C_{A,Init}$  are the influent and initial equilibrium concentrations of the adsorbate,  $t_b$  is the time to breakthrough,  $M_A$  is the molecular mass of the adsorbate,  $\rho$  is the bulk density of the adsorbent, and  $q_A^\infty$  and  $q_{A0}$  are the saturation capacity and initial concentration of adsorbate on the adsorbent (Hines et al 249). Using the parameters for a pipe of 4 in diameter, the minimum length was found to be 37 cm or 15 in (Table 2). This is greater than the length needed to create a sufficient volume to hold the necessary half-daily quantity of silica gel, 11 in. A 6 in diameter section was also considered, resulting in a minimum mass transfer length of 6.5 in and volumetric length of 5 in. Using a wide diameter has the additional benefit of creating a smaller pressure drop across the dehumidifier. However, the column may not perform as well due to the increased likelihood of short circuit paths. PVC pipe in 6 in diameter is also more difficult to find than 4 in pipe, so 4 in pipe was used. It is important to note that the superficial velocity experienced is much less than the superficial fluidization velocity of 2 – 5 mm diameter silica gel beads in air, 0.88 m/s (Hines et al 251).

Concentration of H2O in influent	1.296E-06	mol/cm <sup>3</sup>
Concentration of H2O in equilibrium with initial concentration of solute on adsorbent	1.296E-07	mol/cm <sup>3</sup>
Initial concentration of H2O on silica gel	0.049	g/g
Saturation capacity of silica gel	0.37	g/g
Density of adsorbent	0.72	g/cm <sup>3</sup>
Molecular weight of adsorbate	20.03	g/mol
Time to breakthrough	43200	s
Superficial velocity	0.0856	m/s
Length of stoichiometric wavefront	.3738	m

**Table 2. Calculated desiccation column parameters**

### *Humidifying Column*

Several options were considered for humidifying the gas stream. Commercial products are available that use coaxial tubes with opposing flow of water and air. The

internal tube is Nafion, a material permeable primarily to water, allowing the air stream to become hydrated without gaining or losing any other substances. While these systems can humidify water up to 99% relative humidity, they are both expensive and complex. The additional water reservoir and pump necessary to run the system also decreases the portability of the system.

Instead, a bubbler system is used, consisting of a column of water with an intake tube blowing pressurized air into the bottom of the column and an outlet above the water level. The air is hydrated by water evaporating into the air bubbles as they pass up the column. This process is governed by the Langmuir evaporation rate equation,

$$\frac{dM}{dt} = A(P_{\text{vapor}} - PP_{\text{bubble}}) \sqrt{\frac{M_r}{2\pi RT}}.$$

The partial pressure of water in a bubble is related to the mass of water in the bubble by

$$PP_{\text{bubble}} = \left( \frac{M / M_{r_{\text{water}}}}{M_{\text{air}} / M_{r_{\text{air}}}} \right) P = k \cdot M. \text{ This is a slight simplification, since the pressure in the}$$

bubble will change as it rises through the water column. However, this change is only 8 in H<sub>2</sub>O, or 0.02 atm, so it can be safely ignored. Thus,

$$\frac{dM}{dt} = A(P_{\text{vapor}} - kM) \sqrt{\frac{M_r}{2\pi RT}} = P - QM,$$

an ordinary differential equation with solution

$$M = \frac{P}{Q}(1 - e^{-Qt}),$$

where  $P = P_v A \sqrt{\frac{M_r}{2\pi RT}}$  and  $Q = A \sqrt{\frac{M_r}{2\pi RT}} C$ .

This equation was used with conservatively estimated parameters (Table 3). The mass of water in a bubble, i.e. the relative humidity in a bubble, was found to reach its saturation concentration after less than 0.0001 s (Figure 6). Thus, the air leaving the bubbler should be saturated to near 100% relative humidity for the air and water temperatures involved.

Vapor pressure	3170	Pa
SA bubble	0.000314159	m <sup>2</sup>
Molar mass water	0.018016	kg/mol
Molar mass air	0.02897	kg/mol
R (gas constant)	8.314	J/mol-K
Temperature	298.15	K
V bubble	5.23599E-07	m <sup>3</sup>
Density air	1.168	kg/m <sup>3</sup>
Ambient pressure	101300	Pa

**Table 3. Parameters of bubbler equilibrium equation.**

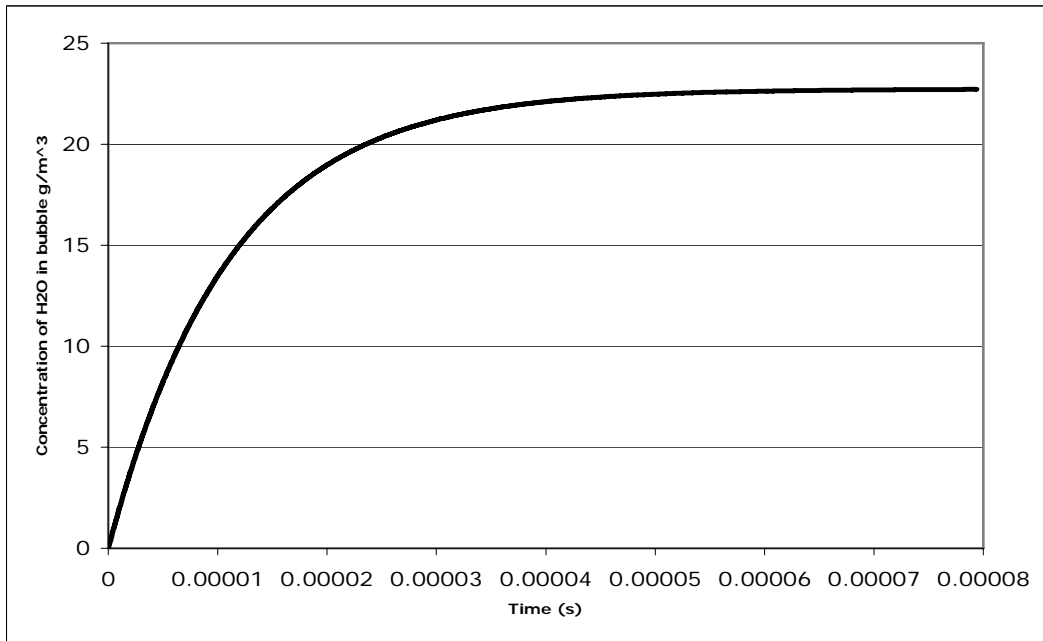


**Figure 6. Time to equilibrium of one bubble.**

Since the mass of water inside the air bubbles equilibrates in less than 1 ten-thousandth of a second, the primary parameter in sizing the humidity control column was the necessary volume of water stored. At any reasonable height of the bubbler, then

bubbles would be fully saturated by the time they reached the top of the column. For ease of construction and connection with the rest of the humidity control system, 3 in PVC pipe was chosen as the bubbler material. At 27 C, 11 gpm, and increase from 0 to 30% relative humidity, 0.46 L/day of water is needed to humidify the air stream. To ensure a reasonable height of water is maintained, the column was sized to hold 0.77 L at 17 cm or 6.7 in tall.

### Sizing of Temperature Controls

To maintain the chamber at a constant temperature, both heating and cooling devices were required to account for all ambient conditions. However, since this chamber is primarily intended for use in the tropics, cooling was the dominant concern. In addition, heating of the chamber by solar radiation will occur regardless of the ambient temperature. The literature suggests that cooling in photosynthesis measurement chambers is a much more significant problem than heating. Thus, only a cooling analysis was completed. The choice of cooling technology, thermoelectric coolers, also made a heating analysis redundant, as discussed below.

The chamber was modeled as an open system using control volume analysis:

$$\dot{Q} - \dot{W} + \dot{m}_{in} \left( h_{in} + \frac{V_{in}^2}{2} + gz_{in} \right) - \dot{m}_{out} \left( h_{out} + \frac{V_{out}^2}{2} + gz_{out} \right) = 0.$$

For the chamber, the only work input is the two mixing fans, which were assumed to draw 2 W. The velocities were found using the 11 gpm flow rate and 2 cm diameter tubes, the enthalpy values of air at given ambient (in) and controller chamber (out) were researched, and the mass flow rate was found using an air density of 1.2 kg/m<sup>3</sup>.

The sources of heat flow into the chamber were considered to be solar radiation, convection from the ambient air, and conduction from the ground. The heat input due to

solar radiation was found assuming the chamber was in San Juan at the hour spanning noon on an average day in July. This situation was both conservative and had readily available solar radiation data. The radiation incident on each of the 5 sides of the chamber was calculated using standard solar energy methods (see Appendix D, the MatLab code for the analysis). Radiation was subtracted both due to the non-unity transmittance of acrylic ( $\tau = 0.9$ ) and the possibility of radiation entering the chamber but being transmitted out another side. The maximum heat input due to solar radiation was found to be 76 W.

The ambient temperature was assumed to be 27 C, the 12 hour average temperature in San Juan in July. The wind speed was assumed to be 20 m/s, a conservatively high estimate. Both free and forced convection were calculated, and the ratio  $\frac{Grashof}{Re^2}$  was used to determine which dominated. If neither dominated, they were assumed to help each other. A laminar analysis was used in both cases, and this assumption was checked and found to be accurate. The heat input due to convection was found to be 29 W.

The ground temperature was assumed to be 30 C, hotter than the ambient air temperature. A standard conduction model was used for this heat transfer. The heat input due to conduction from the ground was found to be 8 W.

Using this analysis, the total cooling power needed was found to be 120 W (Appendix D). Various cooling options were considered, notably thermoelectric coolers (TECs) and Stirling engine heat pumps. All other options, such as standard compression refrigerators, swamp coolers, chemical cooling, and ice buckets, were not practical for field implementation. Volume, weight, and energy draw were all concerns. While

Stirling engines can have coefficients of performance (COPs) as large as 2, this efficiency only exists at large temperature differences. The relatively small temperature difference predicted for the chamber would have driven the COP of a commercially available Stirling engine to fractional values (conservation with Global Cooling rep). These units are also extremely expensive and heavy. In contrast, TECs are generally less efficient than Stirling engines, although their COPs are comparable at the temperature differences expected. They are also much cheaper, lighter, and smaller. Thus, TECs were the technology chosen to cool the chamber. In addition, TECs can both heat and cool depending on the polarity of the voltage across them. This allows for simpler controls for switching between heating and cooling applications.

Due to the large wattage consumed by the TECs, dissipation of the input power is nontrivial. TECs should be placed between two metal sheets, either 1/4" aluminum or 1/8" copper, which are connected to heat sinks (Tellurex sheet). Since the power to be dissipated is at most 240 W from a TEC temperature of 50 C to an ambient temperature of 30 C, the thermal resistance of the heat sinks must be less than  $(50 - 27)/240 = 0.096$  C/W.

### Fluid Flow Analysis

To determine the pressures within the apparatus and the blower power needed, a theoretical internal flow analysis was performed using the Bernoulli equation with losses:

$$\frac{P_1}{\rho} + \frac{1}{2}V_1^2 + gz_1 + GAINS = \frac{P_2}{\rho} + \frac{1}{2}V_2^2 + gz_2 + LOSSES.$$

The assumed losses included both major and minor losses. For the major losses, conservative assumptions regarding the length and roughness of the types of tubing were made (Table 4). The roughness was taken as 0.0015 mm, the value for drawn tubing,

although the tubing was intended to be plastic, which is effectively smooth (Munson 433). The flow rate through the system was assumed to be 42 L/min before IRGA sampling, which was assumed to remove 1 L/min at each sampling location. This assumption, with the assumed diameters, determined the flow velocity through each section. When the Reynolds number in the section indicated laminar flow— $Re < 2000$ —the friction factor was found using  $f = 64/Re$ . When the Reynolds number indicated turbulent flow— $Re > 4000$ —the Moody diagram was used. Reynolds numbers in the transition range were assumed laminar.

Section	Diameter (m)	Overall Length (m)	Velocity (m/s)	Reynolds number	Flow type	Friction factor	Total loss term (J/kg)
Intake	0.06	4	0.25	962	Laminar	0.067	0.14
General	0.02	0.5	2.23	2886	neither	0.022	1.38
Humidity control	0.01	0.2	8.91	5773	Turbulent	0.036	28.60

**Table 4. Major losses assumptions and calculated values**

For the minor losses, plumbing features of the device were assumed and loss coefficients for these devices found (Table 5). The valves were assumed to be fully open globe valves. The total losses packed bed for the desiccant were calculated using the empirical equation

$$F = 1.75u_s^2 \frac{\Delta L}{d_p} \left( \frac{1-\varepsilon}{\varepsilon^3} \right) + 150u_s \frac{\Delta L}{d_p^2} \frac{1-\varepsilon}{\varepsilon^3} \frac{\mu}{\rho},$$

where  $u_s = Q/A$ ,  $d_p$  is the diameter of the particles, and  $\varepsilon$  is the porosity (Table 6). The losses from the humidifying bubbler were assumed to be negligible compared to the desiccant column, so the analysis took the conservative assumption that all flow passed through the desiccant.

Type	Number of fittings	Loss coefficient	Location	Velocity at fitting (m/s)	Total loss term (J/kg)
45 degree joint	4	0.4	General	2.23	4.0
4:1 restriction	3	0.42	Humidity	8.91	50.0
1:4 expansion	3	0.5625	Humidity	8.91	67.0

Entrance	1	1	General	2.18	2.4
Exit	2	0.5	General	2.18	2.4
Valves	3	10	Humidity	8.91	119.2

**Table 5. Minor losses assumptions and calculated values**

Particle diameter (m)	0.002
Height of bed (m)	0.2
Area of bed (m <sup>2</sup> )	0.02
Porosity of bed	0.28
Superficial velocity	0.035
Total losses (J/kg)	140

**Table 6. Dessicant packed bed assumptions and calculated values**

This analysis showed that the blower would need to impart 1.2 W of power on the flow to maintain the given flow rate with the given losses. Using this gain, the gage pressure at the humidity control valves was found to be 1689 Pa, and the pressure at the entrance to the flow meter 41 Pa. These extremely low gage pressures suggested that no specialized equipment for high pressures would be required at any point in the system.

#### Valve Sizing

The  $C_V$  required for the valves was found using the equation

$$C_V = Q \sqrt{\frac{G}{\Delta P}},$$

where Q is the flow rate in gpm, G is the specific gravity of the fluid, and  $\Delta P$  is the allowable pressure drop in psi across the open valve. The pressure drop was conservatively assumed to be 10 psi and the flow rate was 11 gpm, resulting in a  $C_V$  of 0.119. This value was used to guide valve selection, and only valves with equal or larger  $C_V$  values were considered. The low  $C_V$  also helped to identify valves which were overpowered for the system.

#### Leaf Boundary Layer Analysis

Like any flat surface subject to external flow, leaves develop a boundary layer under the action of wind. All gas exchange, including the carbon dioxide and water vapor exchange required for photosynthesis, is limited by the conductivity of this boundary layer, as well as internal resistances. The boundary layer resistance is the only impediment examined here, since the internal resistances vary by species and individual.

The thickness of the boundary layer of a leaf is given empirically by

$$\delta = 4.0 \sqrt{\frac{l}{v}},$$

where the boundary layer height  $\delta$  is in millimeters, the leaf length  $l$  is in meters, and the velocity across the leaf  $v$  is in meters per second (Nobel 364). This equation assumes the leaf is parallel to wind flow. The resistance of the boundary layer to compound  $j$  is given by

$$r_{BLj} = \frac{\delta}{D_j},$$

where  $D_j$  is the diffusion coefficient of the compound (Nobel 397). The literature usually discusses only the boundary layer resistance to water vapor, since if the resistance is acceptable for water vapor it should also be acceptable for carbon dioxide.

The boundary layer should be minimized by maximizing the wind velocity across the leaf. However, sufficiently high velocities will stress the plant, both physically and biologically, and can cause damage. To have a general idea how the air speed would affect the physical integrity of the plant, the plant was modeled as a linear elastic isotropic beam in cantilever bending under a continuous load (Table 7). The plant size was estimated as the average plant size of a specific data set (see Figure 4). The modulus of elasticity was taken as the smallest reported value in a study of the biomechanical

properties of tropical seedlings (Alvarez-Clare). Bernoulli's equation was used to find the pressure at the plant stem. The area of the plant stem was increased by a 1 cm fringe as a conservative estimate of plant surface area perpendicular to the wind. The velocity induced by both the mixing fans and the overall flow rate through the system was conservatively estimated to be the flow rate divided by the entire cross-sectional area of the chamber, resulting in a lower velocity.

Stem diameter (m)	0.007
Stem height (m)	0.2
Force on stem (N/m)	0.134
Modulus of elasticity (MPa)	172
Maximum displacement (m)	0.00132

**Table 7. Biomechanical analysis of plant stem bending**

The maximum acceptable deflection of the stem was taken to be 1 mm to avoid stressing the plant. Using the above analysis, this corresponds with a mixing fan flow rate of 40 cfm, or 0.019 m<sup>3</sup>/s. This induces a velocity of 0.37 m/s across the leaf, resulting in a boundary layer resistance to water vapor of 0.42 s/cm if the leaf length is assumed to be 0.025 m. In a measurement chamber, the boundary layer resistance to water vapor is usually 0.5 to 2 s/cm, although in the natural environment this resistance is usually 0.1 to 0.3 s/cm (Sestak 571-572). The boundary layer resistance generated by a 40 cfm fan is therefore considered acceptable. Due to the large errors possible in this computation, experimentation to find the true boundary layer resistance is necessary. However, this analysis guided the decision to install two 40 cfm maximum flow mixing fans. This allows a large margin of error in case particular plants measured require larger flow rates to reach a sufficiently low boundary layer resistance.

Boundary Layer Calculations

Flow rate (m <sup>3</sup> /s)	0.000683333
Xsect area of chamber (m <sup>2</sup> )	0.0516128
Min avg velocity in chamber (m/s)	0.01323961
Flow rate of fan (cfm)	40
Flow rate of fan (m <sup>3</sup> /s)	0.018877898
Min velocity induced by fan (m/s)	0.36576
Min total velocity across leaf (m/s)	0.365999542
Char length leaf (m)	0.025
Max boundary layer thickness (mm)	1.045417401
Diffusion coeff of H <sub>2</sub> O in air (cm <sup>2</sup> /s)	0.25
Diffusion coeff of CO <sub>2</sub> in air (cm <sup>2</sup> /s)	0.162021861
Min H <sub>2</sub> O conductance BL (m/s)	0.023913893
Min CO <sub>2</sub> conductance BL (m/s)	0.015498294
Max H <sub>2</sub> O resistance BL (s/cm)	0.41816696
Max CO <sub>2</sub> resistance BL (s/cm)	0.645232314

**Table 8. Calculation of boundary layer resistance to water and carbon dioxide**

Diffusion coefficient values are from <http://www.cco.caltech.edu/~brokawc/Bi145/Diffusion.html> and [http://www.jircas.affrc.go.jp/kankoubutsu/jarq/34-1/yoshikawa/34-1\(1-2\).htm](http://www.jircas.affrc.go.jp/kankoubutsu/jarq/34-1/yoshikawa/34-1(1-2).htm).

Density air	1.179174478	kg/m <sup>3</sup>
Pressure at stem	7.897855055	Pa
Stem diameter (m)	0.007	m
Stem height (m)	0.2	m
SA of stem (facing wind)	0.0014	m <sup>2</sup>
Force on stem (N/m)	0.134263536	N/m
Mod. elasticity (MPa)	172	MPa
Moment of Area	1.17859E-10	m <sup>4</sup>
Fracture toughness	1135	J/m <sup>2</sup>
Poisson's ratio	0.33	
Max. displacement (m)	0.001324639	m
Max moment	0.002685271	N-m
Max shear stress	0.026852707	Pa

**Table 9. Calculation of stresses on plant stem**

Stem pressure assumes maximum velocity is 10x minimum velocity. Stem surface area was exaggerated by 1 cm. Mechanics of materials properties of plant stem are from Alvarez-Clare, 2005.

### Mixing

The fans installed to disrupt the boundary layer also function to keep the chamber well mixed, which is vital for accurate measurements and photosynthesis rates. No theoretical analysis of mixing was undertaken due to the extremely complex nature of the mixing process. However, the literature on photosynthesis chambers suggests that chamber flow rates sufficient to lower the boundary layer resistance will also result in a well mixed chamber. This assertion was tested experimentally in the constructed chamber.

### Electrical Signal Calculations

The electrical system is designed to be powered by a portable AC generator producing a standard 120V signal. The energy requirements of the system are shown in Table 10. Since all devices were required to run on DC current at various voltages, power adapters were required. The humidity control valves came with power supplies which required a 0-5 V control signal, deliverable by the LI-6400, and output 0-30 V to the valves, with 0 V being closed and 30 V being open. Both the Peltier temperature control units and the blower require high currents (up to 20A and up to 2A respectively), so a high-current switching power supply was obtained to provide the necessary current. The control voltages required for control of various parameters also varied (Table 11). To satisfy these requirements, the circuit shown in Figure 7 was used (Mancini). The amplifier circuit shown in Figure 7 was also used with no amplification (all resistor values set to the same value) even when the device being read or controlled had 0-5 V input or output in order to buffer all LI-6400 input pins from potential high voltage or high current.

Device	Max Voltage	Max Current	Max Power
Blower	12 V	2 A	24 W
Flow Meter	12 V	100 mA	1.2 W
Sample Pump	12 V	100 mA	1.2 W
LI-6400 (Battery)	NONE	NONE	NONE
RH Sensors (2)	5 V	20 mA	0.2 W
Valves (3)	30 V	400 mA	24 W
Fans (3)	12 V	150 mA	3.6 W
TECs (4)	12 V	5 A	240 W
<b>Total</b>			291.2 W

**Table 10. Power requirements for system.**

Parameter	Control Device	m	b	R <sub>1</sub> (kΩ)	R <sub>2</sub> (kΩ)	R <sub>F</sub> =R <sub>G</sub> (kΩ)	V <sub>ref</sub> (V)
Chamber T	TECs	1.5	7.5	51 kΩ	22 kΩ	51 kΩ	5.4
Bubbler Flow	Valve	1	0	51 kΩ	51 kΩ	51 kΩ	0
Dessicator Flow	Valve	1	0	51 kΩ	51 kΩ	51 kΩ	0
No-Filter Flow	Valve	1	0	51 kΩ	51 kΩ	51 kΩ	0
Flow Rate	Blower	X	X	X	X	X	X
Chamber Mixing	Fans	1.6	4	51 kΩ	22 kΩ	51 kΩ	2.88

**Table 11. Control voltages for output signals.**

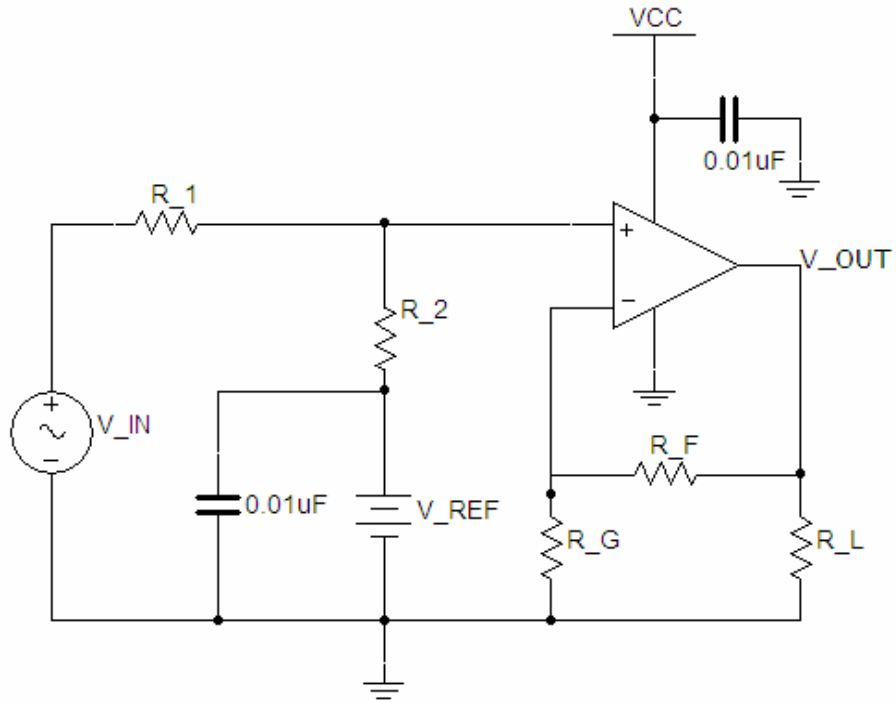


**Figure 7. Amplifier design for inputs and outputs.**

### **System Construction**

The final design for the system is shown in Figure 8. A more conceptual diagram of the system is shown in Figure 9.

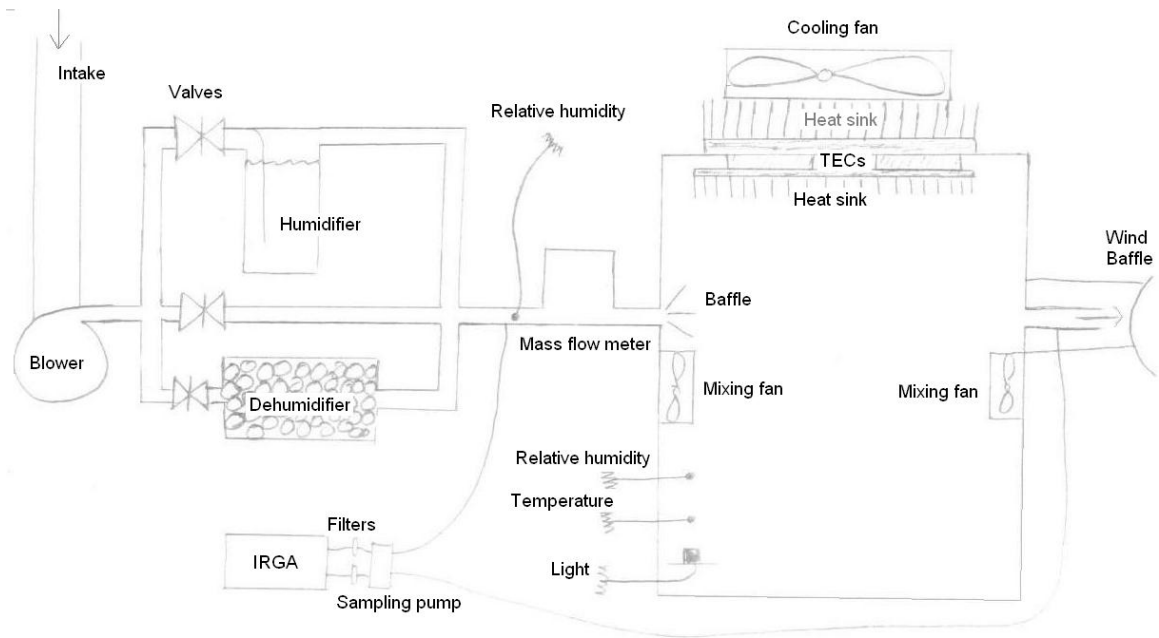


**Figure 8. Final system configuration**

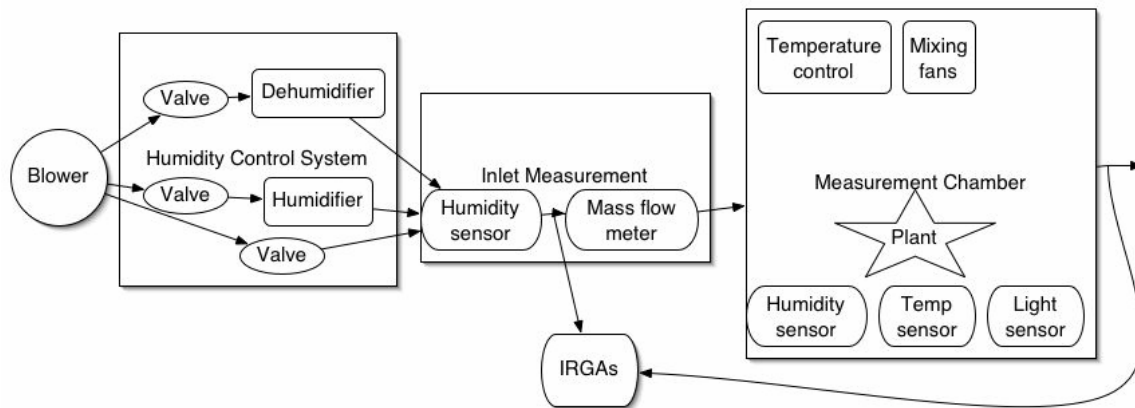


**Figure 9. Final system configuration (conceptual schematic)**

### Sample Collection Subsystem Construction

Air from 1/8" barbs in the initial measurement subsystem and the outlet of the chamber runs through 1/8" Bev-A-Line tubing to two 0.5  $\mu\text{m}$  filters, one for each air stream. These filters were produced with 1/4" male NPT fittings on the ends, so 1/4" female NPT to 1/8" barb fittings were screwed on the filters as adapters. From the filters,

the air passes through more Bev-A-Line tubing to the dual head diaphragm pump. After exiting the pump, the air passes through a final length of tubing before connecting to the IRGA head with 1/8" female swivel brass fittings. The sample collection subsystem is contained in a small, clear plastic box. There are four 1/4" holes drilled to allow the sample tubing in and out of the box, and one number 18 hole to allow the pump wires out.

### Humidity Control System Construction

#### *Humidity Control Columns*

The humidity control columns were both made of PVC pipe. All connections were cemented together using purple primer and PVC cement, except male to female NPT connections. These connections were Teflon taped and screwed in with a wrench. Filled flanges were used as bases rather than caps due to their more stable flat bottoms. The tops of the columns were sealed with plugs and female adapters to allow for replacement of water and silica gel. The inlets and outlets were made of 2" sections of 1/2" PVC pipe. These were installed through holes drilled with a Forsener bit through the pre-cemented adapter or flange and the pipe underneath. Holes were drilled through fittings as well as pipe to allow the inlet and outlet to be as close as possible to the top and bottom of the column. The outer edge between the inlet/outlet pipes and the columns were sealed with silicon caulk.

The humidifying column has the inlet and outlet at the top of the column. Both of these are cemented into 7/8" holes in the sides of the column. On the outside, the inlet has a 1/2" PVC socket to 1/2" PVC NPT female fitting connecting to allow connection to a 1/2" male NPT to barb fitting. On the inside, the inlet connects to a 90° elbow, which

connects to a 1/2" female NPT fitting through an intermediary 1/2" section of PVC pipe. A 1/2" barb fitting screws into this fitting, which has a section of 1/2" ID clear PVC tubing attached. This tubing reaches to 1 cm above the floor of the column to allow the longest path for bubbling air.

The outlet is an open section of 1/2" PVC pipe on the inside. On the outside, it connects to a 1/2" PVC T junction, oriented with the collinear ports vertically opposite. The upper port connects to a 1/2" socket to female NPT fitting via a piece of 1/2" PVC, which connects further to a 1/2" barb and onto interconnecting tubing. The lower port connects to the same series of connectors, ending in another section of 1/2" tubing. This tubing connects to a 1/2" ball valve via another barb fitting. This valve remains shut for most operation. However, if the humidity control unit is jostled and water from the humidifying column goes into the outlet, it will travel down the lower T port rather than the upper one. The valve can then be briefly opened to release the captured water. This system will prevent liquid water from leaving the humidity control system, which could damage the mass flow meter.

The dehumidifying column has an inlet on the bottom and an outlet at the top, allowing the air to flow up through the silica gel (Picture). The inlet and outlet were constructed as for the humidifying column. Due to the larger diameter of the dehumidifying pipe, the drill bit slipped while opening the inlet and outlet holes. The larger holes required additional filling with silicon caulk to ensure an airtight fit. Pieces of wire mesh were attached to the inlet and outlet using Krazy glue to prevent silica gel from leaving the column.

### *Connections in the Humidity Control System*

All fittings are PVC and all connections are glued with purple primer and PVC cement unless otherwise noted. The inlet to the humidity control system is a 1" NPT male fitting, a reducing nipple at 1/2" on the other side. This fitting connects to a 1/2" female NPT to socket fitting, and onto a 1/2" cross via a section of 1/2" PVC pipe. This cross distributes the incoming air flow into three channels: humidify, dehumidify, and do nothing. All channels begin the same way. The cross connects to 1/2" female NPT to socket fittings via 1/2" PVC pipe. These further connect to 1/2" Nylon barb fittings via Teflon taped, screwed male NPT fittings.

After passing through the inlet, air enters the proportional solenoid valves. Clear, 1/2" PVC tubing connects the inlet barb to another 1/2" barb. This barb is screwed into a 1/2" female NPT to 1/2" copper socket fitting. Through a short piece of 1/2" copper tubing, this fitting connects to a 1/2" to 1/4" copper socket<sup>1</sup>. Thin walled 1/4" copper tubing connects from this fitting to a 1/4" compression fitting on the valve. All copper connections were soldered, and then cleaned with acetone. The valve outlet is identical to the inlet.

After passing through the valves, air passes through 1/2" clear PVC tubing to enter humidity altering columns through hose clamped 1/2" barbs. Leaving the column through another barb, the air passes through more 1/2" tubing. The three tubing channels are then brought back together by an identical cross arrangement as in the inlet. The outlet is identical to the inlet.

All the humidity control components are contained in a large, clear plastic tub. The tub has 7/8" holes drilled in the side with a hole saw for the inlet and outlet. This

---

<sup>1</sup> These fittings are difficult to find. They are used almost exclusively in ice makers.

size allows the 1/2" nipple, while on the inside of the box, to screw into the 1" reducing fitting on the outside of the box. The connection between the two parts allows the inlet and outlet to stay in place without securing them permanently with adhesive. A similar technique was used with the water release valve, attached to the side of the box through a 7/8" hole connected to a 1/2" barb fitting. A small hole was drilled with a number 18 drill to allow the valve control wires to pass. All holes were drilled with a hand held electric drill and initially center drilled.

#### Inlet Measurement System Construction

After passing through the humidity control box and before entering the measurement chamber, the air is subjected to a series of measurements. From the 1" female NPT fitting on the end of the interconnecting hose, air enters a 1" PVC female NPT to socket fitting. This connects to a piece of 1" PVC pipe with a hole made with a number 18 drill in it to allow a relative humidity sensor to pass. The PVC section also has a 1/4" male NPT to 1/8" barb fitting screwed into it to allow inlet sample air to be pumped into the IRGA. A 1" PVC socket to female NPT fitting is cemented to the far side of the pipe, which is further screwed into a 1" to 1/4" reducing PVC fitting. Through a 1/4" barb, air passes through 1/4" clear PVC tubing to another 1/4" barb screwed into the mass flow meter. On the far side of the mass flow meter, another set of barbs and tubing routes the air to another 1/4" to 1" reducing fitting. This fitting is screwed into a 1" PVC male to female NPT fitting, which is the outlet for this subsystem.

All these components are contained in a medium sized clear plastic box. Using a hole saw, 1 1/4" holes were drilled in the side of the box, allowing the inlet and outlet fittings to screw into place. A 1/2" hole was drilled to allow the mass flow meter data and

power cable to enter. Finally, a number 18 hole and a ¼” hole were drilled to allow the relative humidity sensor and the sample tubing respectively into the box. All holes were drilled with a hand held electric drill and were initially center drilled.

#### Measurement Chamber Construction

The roof and three walls of the chamber are ¼” acrylic sheet, while the fourth wall and all base pieces are 3/8” acrylic sheet. The thicker wall has the temperature control unit on it, whose weight necessitated using thicker acrylic. The pieces of the upper portion are welded together using acrylic cement. Corner clamps were used to ensure the corners of the chamber were square. Unfortunately, some of the paint from the clamps stuck to the side of the chamber. Sandpaper was used to attempt to remove some of the paint. The chamber walls did not fit perfectly inside the lip, so thicker acrylic cement and clear silicon caulk were used to create an airtight seal. The inside of the chamber was lined with clear Teflon tape after gluing all pieces except the roof square.

The upper portion connects to the base using ¾” 8-32 brass machine screws. The two base pieces are connected using 3/8” 8-32 brass machine screws. Rubber was attached to one side of the lap joint in the base using Crazy Glue. To ensure a smooth joint along glued edges, the base and lip of the chamber were bolted together and end-milled before gluing.

The inlet is a 1” NPT brass nipple to connect to a female swivel fitting on connecting EPDM hose, while the outlet is a 2” section of 1” PVC to allow for the sampling port. The PVC section was turned down on a lathe to closely fit the outlet socket in the chamber wall. Sampled air connects to the 1/8” ID Bev-A-Line tubing

through a 1/4" NPT to 1/8" barb fitting screwed into the side of the PVC section. The outlet is protected from incoming wind by a wind incursion baffle constructed from a section of 4" PVC pipe connected to the side of the chamber by 4" 10-32 brass machine screws. It attaches to the chamber through holes tapped in the side of the chamber.

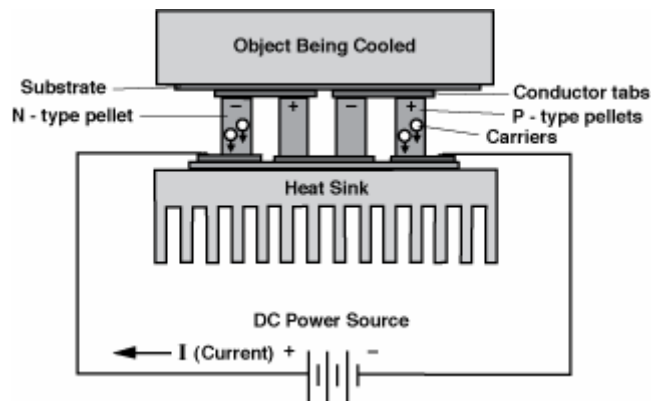
All holes were made on a drill press using dubbed bits to avoid cracking the acrylic. All taps were done by hand except the 1" NPT tap for the inlet and the 3/4" tap for the TEC sealing gland. Those taps were done with the aid of a milling machine to ensure a vertical tap. The cemented edges of acrylic were milled smooth on a Bridgeport milling machine before welding for the best possible seal. The rectangular hole for the temperature control unit was milled on a Bridgeport as well. The corners of the hole remained rounded to avoid reentrant corners leading to weakened material.

The wires for the TECs pass through an Altech model 4220802 sealing gland, for cables 8 to 16 mm in diameter. All other wires pass through two Altech model 4220712 sealing glands, for cables 1.5 to 5 mm in diameter. One is exclusively for the quantum sensor, while the other allows the bundled fan, RH sensor, and thermocouple wires through the chamber wall.

#### Temperature Control Unit Construction

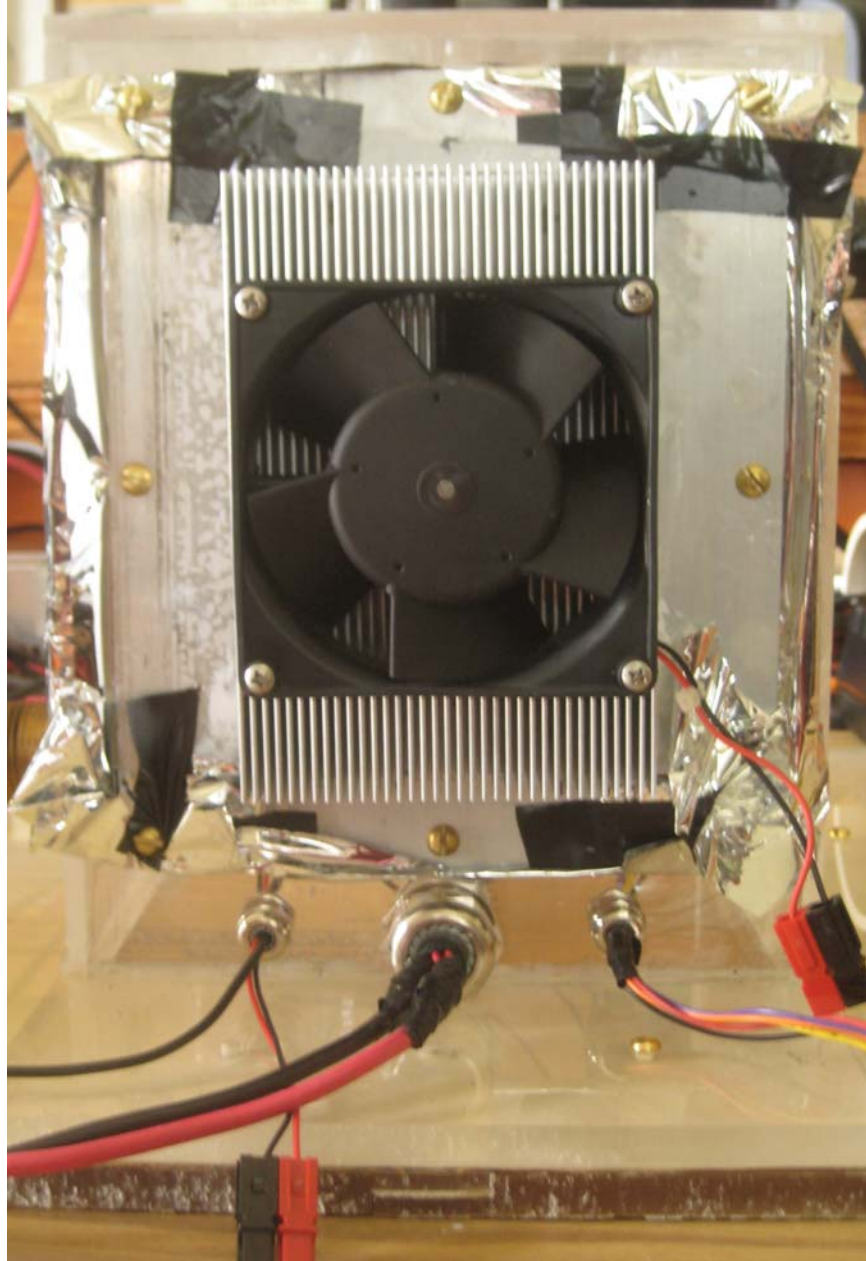
The temperature control unit consists of the TEC units, a 1/4" aluminum mounting plate, and two heat sinks (Figure 10). The mounting plate has a 1/8" step cut into it to allow the TECs to lie closer to the center of the chamber. The lip is lined with 1/16" rubber sheet to reduce gas transfer. The mounting plate connects to the chamber with 8 clearance holes connecting to 10-32 tapped holes in the chamber wall via 1/2" brass machine screws. Strips of 1/16" rubber sheet were glued to the edge of the mounting

plate with aerosol (spray-on) adhesive. This bond is not assumed to be permanent, but was made to test the performance of the rubber. Both the inner heat sink and the mounting plate have clearance holes to allow 1" brass machine screws to reach tapped holes in the outer heat sink. These machine screws hold the entire unit together, including providing light compression on the TECs to keep them in place. The outer cooling fan attaches to the heat sink with 2" long 6-32 brass machine screws into tapped holes in the outer heat sink.



**Figure 10. TEC schematic (our setup had heat sinks on both sides and used a PWM power source rather than DC)**

To avoid damaging the heat sinks, all holes were drilled from the unfinned side of the heat sinks on a drill press. To allow space for screw heads, larger holes were milled out of the finned face using a Bridgeport milling machine and flat-bottomed endmill bits. Since the unfinned bases of the heat sinks were slightly thicker than 1/4", an additional metal plate on the inside was considered unnecessary. Consideration of the added weight and volume inside the chamber led to the use of only the heat sink on the inside.



**Figure 11. Exterior of TEC Assembly**

The heat sinks used are H.S. Marston 890SP-01500-A-100 extruded aluminum heat sinks (Ref to spec sheet). These have a rated thermal resistance of 0.08 C/W when used with one Papst 3312 fan (Ref to spec sheet). The outer heat sink, which will be hot when the chamber is cooled, has an attached Papst 3312 fan. The inner heat sink does not have an attached fan, since the air circulating fans are considered sufficient. The

TECs are not anticipated to be used for substantial heating of the chamber, so the inner heat sink will not be used to dissipate comparable heating loads.

### *Critical Components of Control and Measurement System*

The primary control and measurement components in this system are the blower, the control valves, the mass flow meter, and the sampling pump. Crucial electrical and control components were a high-current power supply to provide power to the TECs and the blower, a controller for the TECs, and suitable operational amplifiers for voltage scaling circuits. All of these components were both expensive and required particular care in selection to ensure a functional complete system.

### *Blower*

The combination of 11 gpm flow and at least 0.18 psi pressure (see fluid flow analysis) is an uncommon specification. Fans do not offer sufficient pressure, and most blowers do not operate at sufficiently low flow rates. The Ametek 3" Microjammer blower, part 119349-51, delivers 11 gpm at the correct pressure range (See spec sheet, attached in Appendix G). This blower uses input voltage as speed control. The blower outlet fits 5/8" ID tubing. The inlet is a 1.25" opening in the side of the blower to allow air to enter.

### *Control valves*

The control valves used are Aalborg PSV15-VA proportional solenoid valves. These valves can easily withstand the pressures required in the system, having a Cv of 0.24 and a maximum air flow of 100 L/min. A control voltage is processed by the Aalborg PSV-D driver module and converted to an active voltage. This active voltage energizes the solenoid to lift a bar, allowing flow, and higher voltages lift the bar further,

allowing more flow. Although solenoid valves generally come in both normally closed and normally open models, proportional solenoid valves are only available in the normally closed option. A power input is required for any valve to be open, even if the degree to which it is open does not change. This power consumption is a disadvantage over other kinds of proportional automated valves, such as globe valves with servo motor controls. However, these valves are not available in the small sizes required for this system.

### *Mass flow meter*

The flow meter used is a FloCat M Series 100SLPM model mass flow meter. The device is fundamentally a volumetric flow meter, since it takes differential pressure readings to calculate the flow through a laminar flow element. However, since the device also takes temperature readings, this volumetric flow can be converted to a mass flow as needed. Both the mass flow and the temperature readings are sent as output to the LI6400. Since the mass flow rate through the chamber is used directly in the calculation of photosynthetic rates, an accurate mass flow meter is required. With an accuracy of +/- 1%, this flow meter is extremely accurate. A model with maximum flow of 100 L/min was chosen to allow for a range of chamber air turnover rates while maintaining accuracy at the expected flow rate of 42 L/min.

### *Sampling pump*

The sampling pump is a Hargraves model D771-11 parallel diaphragm pump designed for air, providing up to 2.8 L/min in parallel. The pump will be operated as two separate pumps, drawing the inlet and chamber samples at 1 L/min. A parallel pump was chosen so the same motor ran both pumps, ensuring the flow rate and pressure in both

sample lines is as similar as possible. This similarity is required for the IRGA to make correct readings, since differences in the pressure within the analyzer chambers can distort measurements. Using a diaphragm pump decreases the likelihood of sample contamination from the pump.

### *Electrical Components*

In order to supply power to the TECs and blower, a high-current power supply was needed. A switching-mode power supply was selected for its light weight. The specific power supply chosen was a Twinfly power supply yielding twelve volts at 26.5A. Also necessary for the TECs was a method of controlling supplied power. A dual op-amp circuit was considered but rejected in favor of a pulse-width modulation (PWM) controller. A TETech TC-36-25 RS232 thermoelectric cooler temperature controller was chosen for its ability to handle currents of up to 25A (a maximum of 20A will be required for the TECs) and its optional control input.

The op amps used for the low-power buffering circuits were Linear Technology LTI1490 rail-to-rail op amps. The op amps used for the blower control circuits were Texas Instruments TLV4110IP amplifiers. High-power resistors were used in the circuit to ensure that there would be no component failure.

### *Programming on the LI-6400*

The LI-6400 allows for two levels of programming. The lower level is LPL, which permits the user to construct a program for the machine essentially from the ground up, including button responses, figures displayed (including all display parameters), analog input and output responses, and so forth. It was initially thought that this high degree of control would be necessary for the project, but it was found that the

higher-level operating system could be used to control as desired with little loss of flexibility. The higher level is OPEN, the operating system run by default on the LI-6400. There are two locations in which OPEN parameters were changed. The configuration file was changed to add the analog input pins which provide information on temperature, flow, and humidity. In order to process this information and output the appropriate control voltages, the ComputeList was edited (see Appendix E for this code).

## **Testing**

### *Blower Compatibility Problems*

The blower was sized using internal flow analysis that neglected the pressure drop across the mass flow meter. This pressure drop was assumed to be negligible. In fact, the drop is approximately 2.5 psi in the meter specification, while the pressure drop across the system otherwise was predicted to be less than 0.5 psi. This oversight resulted in the purchased blower being incompatible with the flow meter. In addition, the blower was undersized to handle the actual pressure drops across the humidity control system. Due to the construction constraints, the actual system had more turns and longer lengths of small tubing than predicted, again resulting in a higher pressure drop.

The problem was detected when substantially smaller flows than expected were observed by the mass flow meter when running the blower at 12V as specified. Initially, the problem was assumed to be a broken blower, since a pump curve of the blower produced using the mass flow meter did not match the specified curve (Figure 12). The blower was exchanged, and the same problem was observed. After the true cause of the problem was found, a volumetric flow meter with an actually negligible pressure drop was calibrated against the mass flow meter for use in testing subsystems. A system curve

was developed using the volumetric flow meter to help size a new blower that is compatible with the system as is.

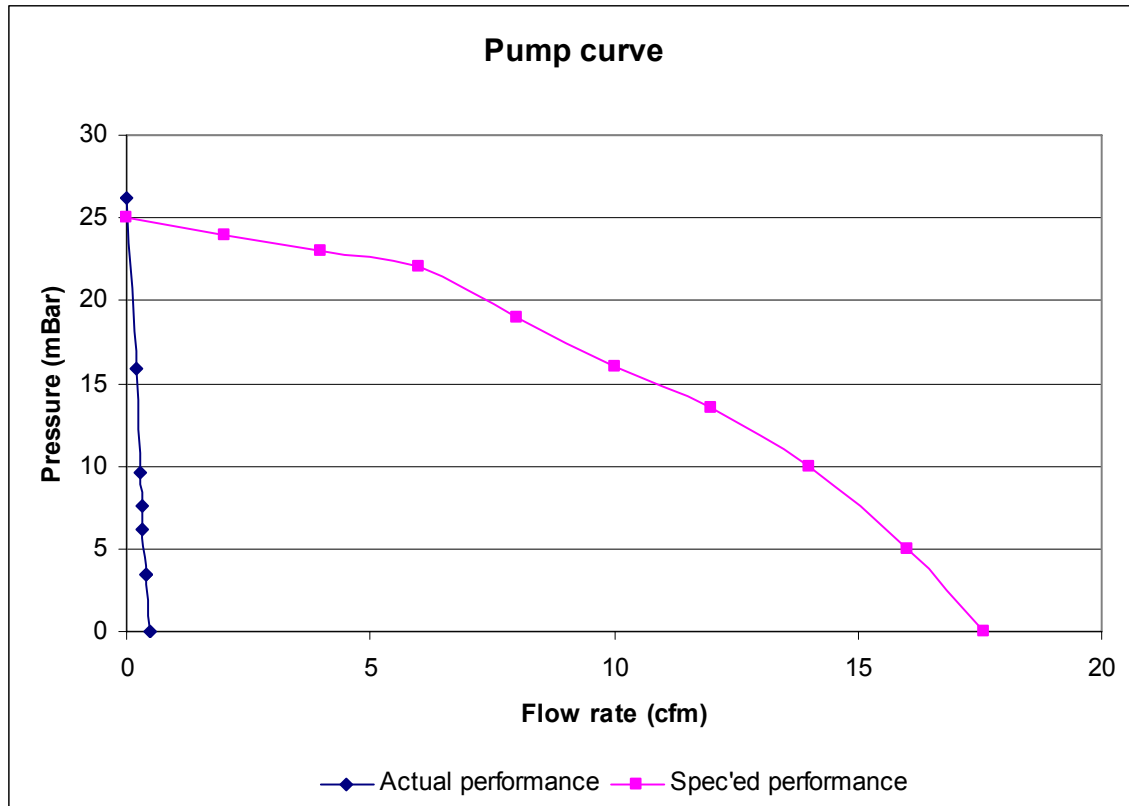


**Figure 12. Pump curves: specified and measured with mass flow meter.**

#### Calibration of Volumetric Flow Meter

It was important to have a method of measuring flow to ensure that flow rates through tested subsystems were similar to the design flow rate of 42 L/min. After discovering the large pressure drop across the mass flow meter, a rotameter type volumetric flow meter was calibrated against the mass flow meter for use in testing. The volumetric flow meter was connected downstream of the mass flow meter using rubber hosing. The voltage across the blower was then varied to achieve a range of flow rates through the system as measured by the volumetric flow measurement feature of the mass

flow meter (Figure 13). The calibration found was piecewise linear. For readings less than 2.5,  $F = 2.7605R + 4.382$ ; for readings greater than 2.5,  $F = 3.8063R + 1.0851$ ; where  $F$  is the flow rate in L/min and  $R$  is the reading of the rotameter. An additional calibration run can be found in Appendix F.

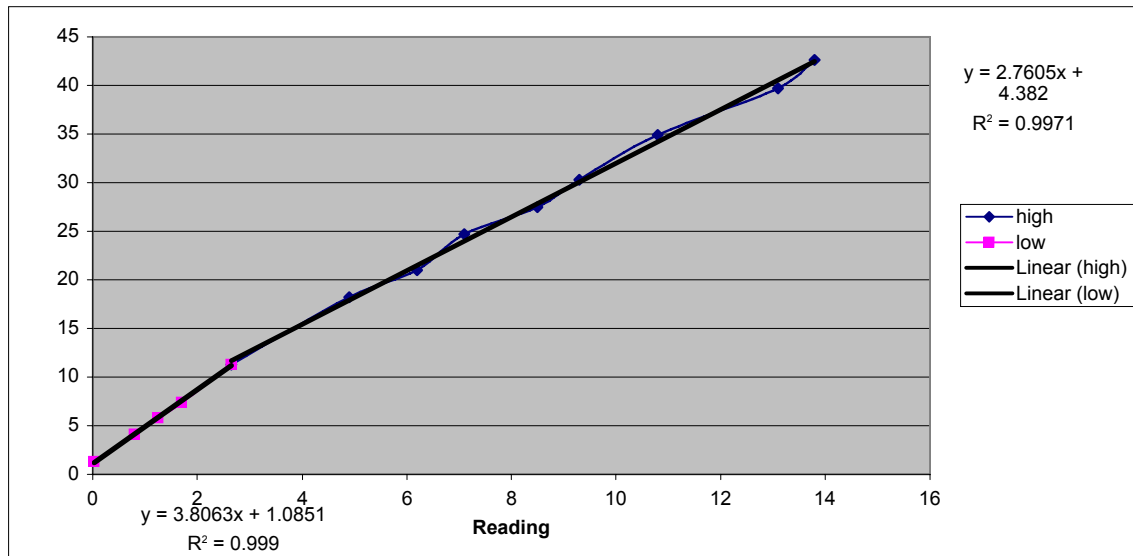


**Figure 13. Calibration of volumetric flow meter against mass flow meter.**

### System Curve Test

To aid in the selection of an appropriate blower, as well as to test the flow characteristics of the built system, an overall system curve was found. Since the blower available could not force air through the entire system, even when subject to 210 W of power input compared to its rated 24 W, the curve was obtained by combining the curves for each component. Each component curve was found by measuring the pressure and flow at the blower outlet while varying the power input to the blower. The pressure was measured in a U-tube manometer filled with blue oil (s.g. = 1.75) and the calibrated volumetric flow meter was used to find the flow rate. The volumetric flow meter was attached to the component by one of the rubber hoses. Power curves were found to be

reasonable approximations of each component curve and were fit to each data set using Excel (Figure 14). The best fit curves of each data set were then added to form the composite system curve (Figure 15). Since all components were not tested at exactly the same flow rates, test results could not be added directly. Additional component test results can be found in Appendix F.

Several details are important to note. Many of the component tests do not have a data point for flows near 42 L/min. Tests were run for as high a flow rate as the blower could reasonably sustain. At high power levels, the blower emitted highly variable flow, so good readings were not possible. In addition, the power supplies to the humidity control valves could only supply enough power to put 20 V across them, meaning the valves were only 2/3 open. If the valves were fully open, a lower pressure drop would result. Secondly, the composite system curve has the summed component curves for the initial measurement box including mass flow meter, the blank line of the humidity control system 2/3 open, the humidifying line 2/3 open, and the chamber. The interconnecting hoses are included by the necessary hose connecting the flow meter to the component in each test. This was considered a conservative curve, since the pressure drops from two lines are added, the valves were only 2/3 open, and the bubbler has the largest drop of the three lines. Sizing a blower on this curve should ensure it can produce 42 L/min through the system under any configuration. Often, less power to the blower will be needed, so a variable speed blower will be purchased. Finally, pressure drop across the volumetric flow meter was subtracted from all data to create the individual and composite system curves.

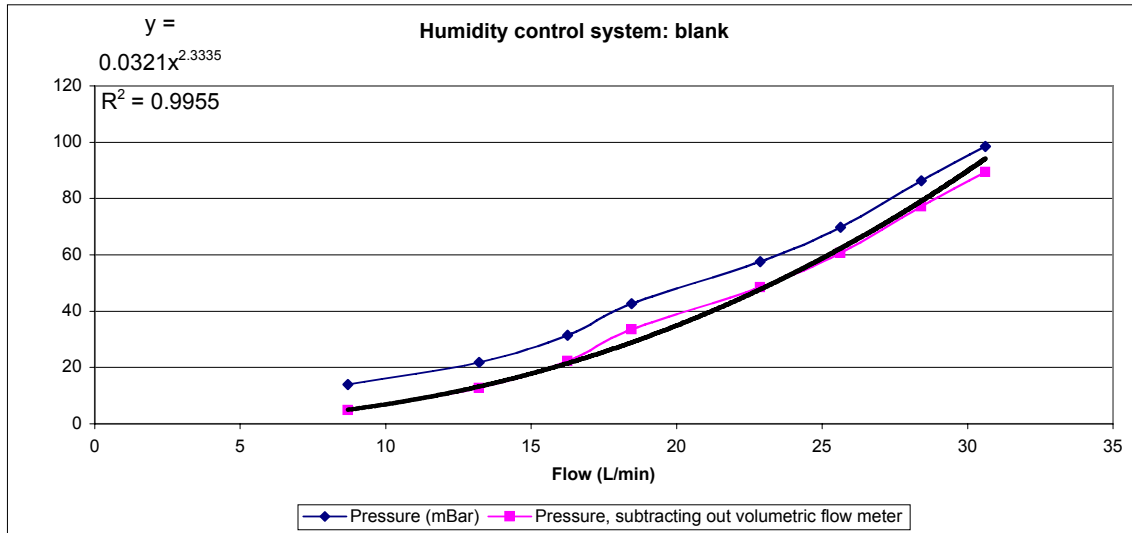


**Figure 14. Results from testing the blank line of the humidity control system.**

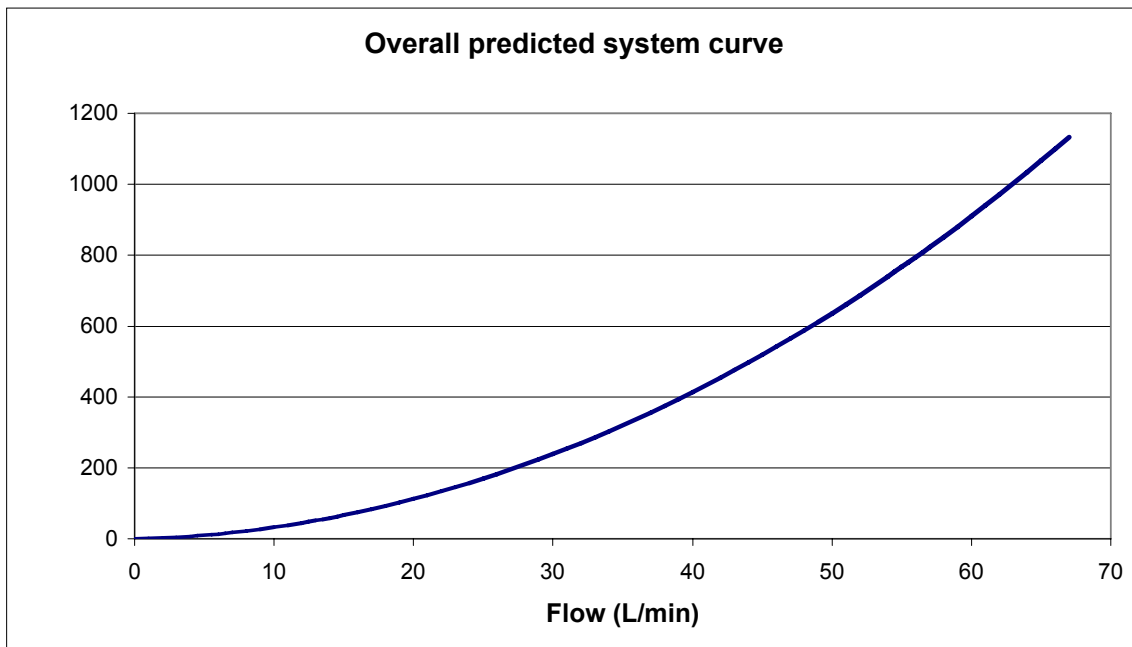


**Figure 15. Overall system curve. Smooth because it is a combination of individual best fit power curves.**

Chamber Mixing Test

The air at the outlet of the chamber is assumed to be representative of the air inside the chamber for photosynthesis calculations. While the homogeneity of the carbon

dioxide and water vapor concentrations within the chamber are of direct interest, equipment to measure these concentrations at multiple points inside the chamber was not available. Thus, the distribution of heat was used instead of gas concentrations to test chamber mixing. Thermocouples were placed in four locations within the chamber—inlet, outlet, quantum sensor, and plant level—and the measured temperatures at each location recorded as they changed with time due to a heat input. In the first tests, the input was a hairdryer at the blower intake. However, this arrangement did not adequately simulate the actual functioning of the chamber. A plant inside the chamber was the intended source of gas concentration change, not any source at the blower intake. Later tests were conducted with a heat source internal to the chamber at approximately plant level. The heat source used was a 5V voltage regulator connected to 6 – 9 V. All tests were run at approximately 42 L/min flow as measured by the volumetric flow meter. These tests were conducted independently of other subsystems, and all devices were run from power supplies.

The results of these tests show the temperature inside the chamber increasing with time (Figure 16). The temperature at each point began slightly different, indicating temperature differences already existed in the chamber. The temperatures at the plant and quantum sensor are generally larger than the temperatures at the inlet and outlet. However, the difference between the temperature at a given time and the initial temperature is more consistent. This difference is similar at all points except the plant, which is consistently larger. These results indicate that changes at the plant level take time to transfer to the rest of the chamber. However, away from the plant, the air in the

chamber is generally homogeneous. Mixing in the chamber is therefore fairly good, but could improve to mix air from next to the plant into the rest of the chamber more quickly.

QuickTime™ and a  
decompressor  
are needed to see this picture.

QuickTime™ and a  
decompressor  
are needed to see this picture.

**Figure 16. Results of one mixing test in which 9 V were placed across the 5 V voltage regulator.**

#### Light Loss Tests

Due to the large volume of auxiliary equipment inside the chamber, it was not obvious that the light at the plant level was the same as the light measured by the quantum sensor. In addition, the Teflon tape coating, while nominally clear, was visible. The coating could cause light loss, resulting in the plant receiving less light than was available. These scenarios were tested by using additional quantum sensor placed at

plant level and outside the chamber. . In these tests, the chamber was oriented with the blank wall to the south, as intended. The readings of these sensors were compared to the installed quantum sensors (Table 12). The recorded numbers are raw output from the sensors and are not converted to a meaningful light measurement The installed sensor reads always 5 or 6 units less than the secondary sensor, even when the secondary sensor measures precisely the same location. This difference is therefore due to differences in sensors rather than light exposure. These results show that the light at plant level is effectively the same as the light at the quantum sensor and that no measurable light loss occurs through the chamber walls.

Reading		
Internal quantum sensor	External	Which external
94	99	plant level inside chamber
94	99	on top of other QS inside chamber
94	100	above other QS outside chamber

**Table 12. Light loss test results.**

### Temperature Control System Tests

The temperature control system did not function as intended. Performance was tested using the software provided by the controller manufacturer, which logged the set temperature, the actual temperature, and the percent total possible power directed to the TECs. The RTD measuring actual temperature was set in the chamber near the cooling side heat sink. The first tests showed the coolers to initially function well, lowering the temperature inside the box (Figure 17. Initial test of TEC performance, without modifications.). However, the temperature eventually begins rising despite continued operation of the coolers. The temperature rises more sharply after the TECs are deactivated. Note that since the TECs are cooling, the power is negative. Note also that

the controller gives out power proportional to the difference between the actual temperature and the set temperature relative to a bandwidth. The smaller the bandwidth, the closer the actual temperature needs to be to the set temperature for the controller to start reducing the power directed to the TECs.

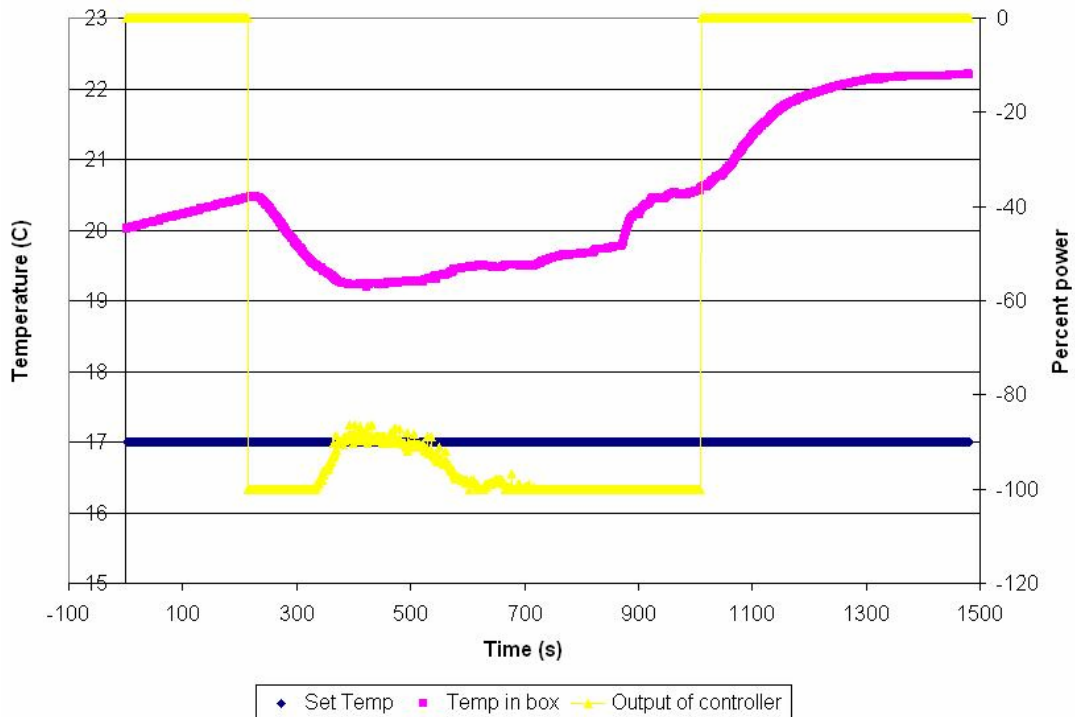


**Figure 17. Initial test of TEC performance, without modifications.**

It was determined this behavior could be due to two compounding effects. First, the heat pumped through the TECs could leak back into the chamber. Second, the heat dissipation from the hot side heat sink and fan could be insufficient. The heat leakage explains why the temperature began to rise despite continued TEC pumping, and the insufficient dissipation explains why the temperature continued to rise without reaching an obvious steady state. Various techniques aimed at improving heat dissipation were attempted, including additional fans blowing across ice buckets and increasing the power to the existing fan (Appendix F). None had any observable effect.

To reduce heat leaking, mylar strips were taped into place along the edge of the aluminum plate in contact with the inside of the chamber. When the heating assembly was taken off the chamber to perform the installation, it was discovered that the TEC units were loose and could be wiggled between the inner heat sink and the aluminum plate. Thus, the heat sink assembly screws were tightened, with care to not damage the TECs. While the cooling unit was disassembled, more thermal grease was applied between the plate and the external heat sink to give a more uniform coating. These adjustments lead to a marked improvement in performance (Figure 18). The set point was still not reached, and the temperature began to increase again, but to a much lesser extent. Note that the power to the TECs was 100% for the entire run, indicating that the increase in temperature could not have been prevented by increased pumping by existing units. The improvement is likely due to the improved thermal contact between all components of the system, allowing the heat generated by the TECs to move more easily to the heat sinks and on to the environment. The addition of mylar insulation led to further improvements in performance in one test. The set temperature was still not reached, but a steady state was achieved (Figure 19). The surface temperature of the plate was observed to be 109.4°C while the heat sink was 105.6°C, indicating good thermal contact between the two components. However, in later tests, a reversion to the original behavior was observed (Figure 20).

Upon observation of this reversion, new adjustments were made. More mylar was added, with no observable effect. A heat dispersion fan was installed on the internal, cool side heat sink, again with no observable effect. Without success, the addition of foam weather-stripping on the inside was installed. Multiple tests were run varying the

difference between the set point and the initial actual temperature, as well as the bandwidth, to see if any such combination resulted in a functional cooling system, with no success. The temperature at the heat sink and multiple points inside the chamber were monitored during the same test run, with results indicating good heat transfer between the chamber and the inner heat sink. The output of the controller was tested as well. When the computer software reported 100% power output, testing with a multimeter showed 12 V across the leads and 15 A going through them, as expected. In addition, a test was run with a higher than ambient temperature, and the TECs were found to achieve the set point and maintain it. Thus, the controller was found to be functioning properly. Detailed results from these tests are available in Appendix F.

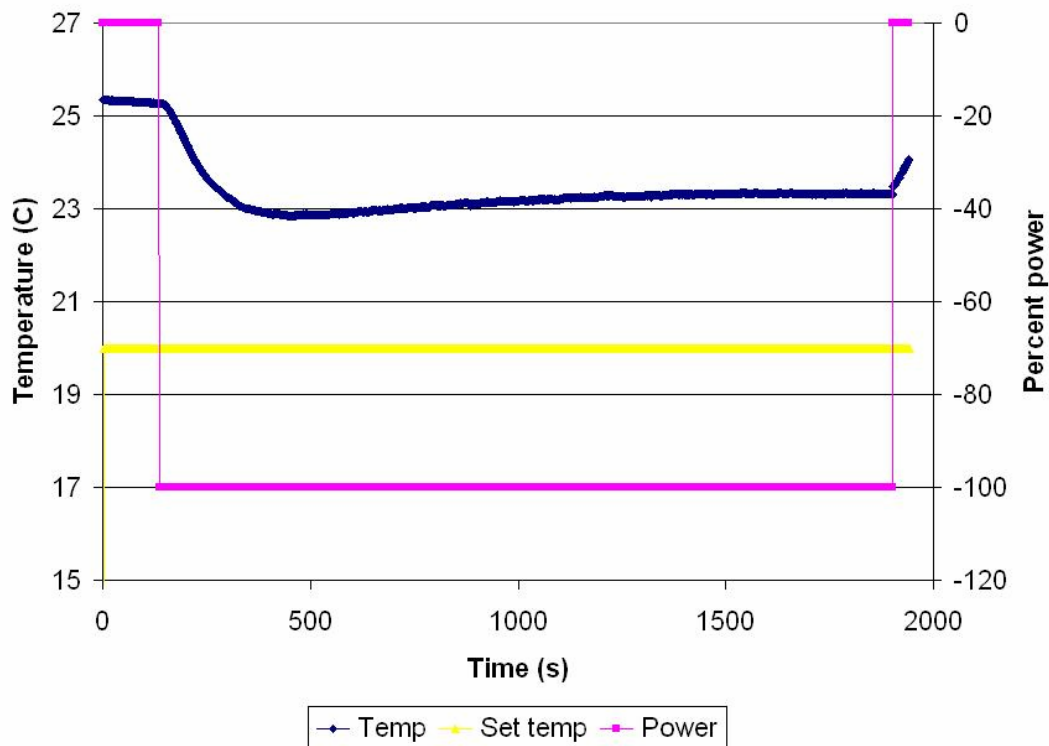


**Figure 18. TEC performance after tightening and regreasing.**

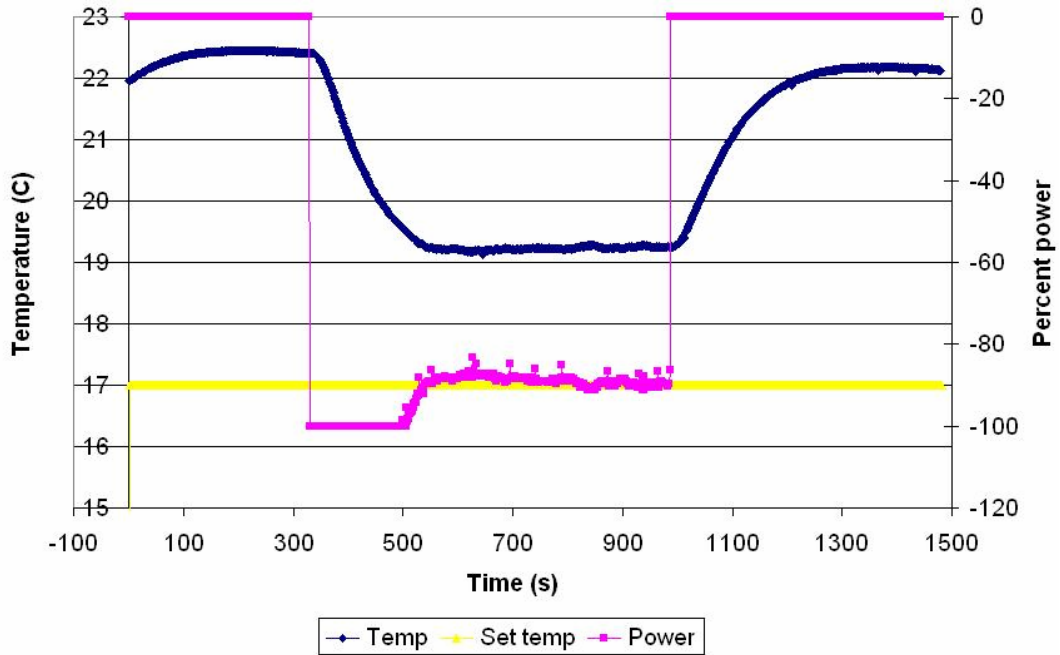


**Figure 19. TEC performance after first layer of mylar insulation.**

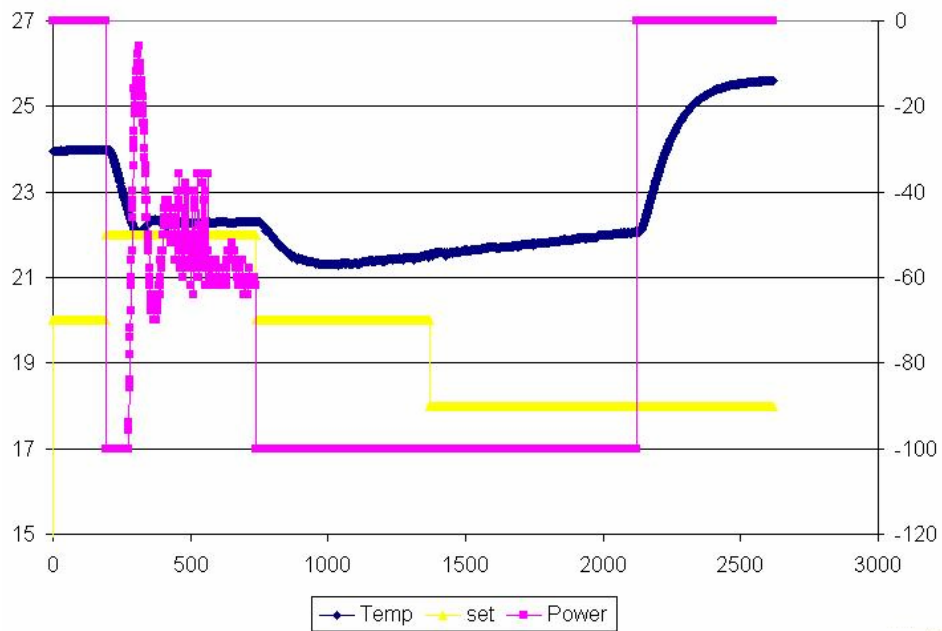


**Figure 20. Reversion to previous poor performance.**

Gas Exchange Test

Since the system measures photosynthetic rates by plant gas exchange, it is assumed that the only gas exchanged measured is due to the plant. This assumption was

tested by analyzing samples before and after the chamber with no plant inside. Two tests were run: one with blower intake air at ambient conditions and one with increased carbon dioxide and water vapor. The first run would show if the IRGAs were matched properly, since no gas exchange at all was expected between two volumes with gases at approximately equal concentrations. The second run would show diffusion of gas from the increased concentration inside the system to the environment if any existed. The increased concentration of carbon dioxide and water vapor at the blower was achieved by the tester breathing near the intake. The LI6400 took recorded readings from the IRGAs every 10 seconds for 40 minutes for each test. Unfortunately, the data link between the LI6400 and the computer was not operational at the time of the test, so the data was manually transferred to the computer.

The results suggest that no gas exchange occurred in either run (Figure 21, Figure 22). No observable difference between the pre- and post-chamber carbon dioxide concentrations is visible in the ambient run. The water vapor measurements have a constant offset in this test, indicating poor IRGA matching. This test was run after the match valve control on the IRGAs began malfunctioning, so repeat tests with matched IRGAs were not possible. For both carbon dioxide and water vapor measurements in the increased concentration run, the reading at the chamber outlet lagged readings before the chamber. However, the graphs eventually reached approximately the same height, indicating no gas exchange occurred.

QuickTime™ and a  
decompressor  
are needed to see this picture.

QuickTime™ and a  
decompressor  
are needed to see this picture.

**Figure 21. Results of gas exchange test for carbon dioxide.**

**The top graph is with ambient conditions at the intake, while the bottom graph shows increased carbon dioxide concentrations at the intake. The “R” designation stands for “reference” or pre-chamber, while “S” is “sample” or post-chamber.**

QuickTime™ and a  
decompressor  
are needed to see this picture.

QuickTime™ and a  
decompressor  
are needed to see this picture.

**Figure 22. Results of gas exchange test for water vapor.**

**The top graph is with ambient conditions at the intake, while the bottom graph shows increased water vapor concentrations at the intake. The “R” designation stands for “reference” or pre-chamber, while “S” is “sample” or post-chamber.**

Volumetric Leak Test

The chamber was tested for volumetric leaks of air. Approximately 42 L/min air was forced through the chamber and one hose, as measured by the volumetric flow meter. The outlet of the chamber was then covered and the continuing flow recorded (Table 13). The remaining flow was assumed to be indicative of leaks during normal operation, although larger due to the larger pressure inside the chamber. Initially, there was approximately 3 L/min of leaks. After taping and caulking over several observed leaks, the leak flow dropped to 0.1 L/min, which is approximately 0.2% of the total flow. This was considered acceptable, especially considering the open system design of the chamber.

	Run 1		Run 2		Run 3, next day		
	Initial	Sealed	Initial	Sealed	Initial	Sealed	Sealed w/ fan holes tacked
Reading	14.3	0.1	13.8	0.1	13.6	0.4	0.4
Flow (LPM)	43.85715	1.46573	42.4769	1.46573	41.9248	2.60762	2.60762

	Run 4, no more tack		Run 5, after taping leaks	
	Initial	Sealed	Initial	Sealed
Reading	14.1	0.5	14	-0.25
Flow (LPM)	43.30505	2.98825	43.029	0.133525

**Table 13. Results of leak testing.**

Humidity Control Column Test

The ability of the humidity control columns to alter the relative humidity of the incoming air was tested in isolation from the rest of the system. Voltage sources were used to put 20 V across one control valve at a time, opening it to approximately 2/3 open. The voltage sources available could not provide 30V to fully open the valves at the required current. The initial tests were run with the blower at 12 V, resulting in a lower

flow rate through the system than intended (Appendix F). Later tests were run at measured flow rates (Table 14). The dehumidifying column was tested with saturated input air by placing the blower inlet near a standard room humidifier. A similar test was intended for the humidifying column by dehumidifying the room, although the lowest room humidity was only near 30%. At all measured flow rates, the humidity controlling columns functioned as intended.

The first time flow rates comparable to design through the humidifying column were used, the water in the column bubbled so high it passed through both the inlet and outlet to adjoining tubing. While the emergency drain functioned initially, it soon filled. The water level in the bubbler was then lowered slowly by absorption onto a towel until the bubbles no longer caused flooding. According to this test, only 3.25” water should be placed in the column to avoid flooding other lines. This flooding occurred before the tabulated test run. The remaining moisture in the no change line is the likely cause of the increasing relative humidity in the blank column.

**Blank column, no change**

Flow reading	Flow rate (L/min)	Relative humidity
0	0	56.6
9.9	31.71095	57.1
6.4	22.0492	57.4
4.6	17.0803	57.7
2.6	11.5593	58.8

**Dehumidify, humidified air**

Flow reading	Flow rate (L/min)	Relative humidity
0	0	102.7
9	29.2265	9.1
6.4	22.0492	9
5	18.1845	9
2.5	11.28325	10.9

**Humidify, dehumidified air**

Flow reading	Flow rate (L/min)	Relative humidity
--------------	-------------------	-------------------

0	0	33.9
9.5	30.60675	102.7
6.2	21.4971	102.7
4.5	16.80425	102.7
2	9.903	102.7

**Table 14. Humidity test results at known flow rates.**

**Future Work**

The system currently has two major problems. First, the temperature control system does not function properly. Further experimentation is required to further diagnose and repair the unit. Planned tests include applying thermal grease to both sides of the TEC units to increase heat conduction to the sinks. This solution was not originally considered because the TECs have a factory-applied conductive coating. However, this coating may be insufficient for the current application. If necessary, different heat sinks will be tested, as well as more powerful fans. Different insulators may be used, including applying insulation in the void space between the TECs.

The blower is not currently compatible with the rest of the system, notably the mass flow meter. However, the pressure drop across the humidity control system is also larger than predicted, due to the longer lengths of small diameter tubing and larger numbers of changes in flow direction than originally assumed. Thus, a new blower will be bought, using the true system curve for sizing. It may also be possible to buy a mass or volumetric flow meter with a smaller pressure drop. Thermal mass flow meters generally have smaller pressure drops than the differential pressure meter currently in use. These were originally discarded due to the temperature control desired elsewhere in the system. However, the heat input may be negligible compared to the cooling required. Momentum flow meters, such as turbines, are generally less accurate than the above

models and thus were rejected. While further research in this area may result in the requirement of a less powerful blower, a new blower is needed in any event.

In addition, many smaller problems must be resolved before the system is fully operational. Further electrical connections must be made. A problem with communication between the computer and the LI6400 must be resolved. The LI6400 also currently continually blows a fuse, which LICOR has identified as a short in the circuit board requiring company repair. Power supply to all components must be finalized. Electronic circuitry must be mounted in waterproof containers. To obtain more uniform inlet carbon dioxide levels, a system for taking inlet air from 4 m above the tree line should be constructed. The simplest way currently envisioned is the use of a telescoping radio antenna mast to hold wide diameter flexible tubing than runs down into a small buffer volume feeding the blower. This work is intended to be carried out by the authors within the month.

## References

- Alvarez-Clare, Silvia. 2005. "Biomechanical Properties of Tropical Tree Seedlings as a Functional Correlate of Shade Tolerance." University of Florida.
- Agata, Waichi; Hakoyama, Susumu, and Kawamitsu, Yoshinobu. 1985. "Influence of Light Intensity, Temperature and Humidity on Photosynthesis and Transpiration of *Sasa nipponica* and *Arundinaria pygmaea*." *The Botanical Magazine, Tokyo* **98**: 125 – 135.
- "Configuring and Operating the LI-6400 Portable Photosynthesis System with External Sensors." *Application Note: LI-6400 Portable Photosynthesis System*. Vol 1. LI-COR, Inc.
- Corelli-Grappadelli, Luca and Magnanini, E. 1993. "A Whole-tree System for Gas-exchange Studies." *HortScience* **28(1)**: 41 – 45.
- D'Souza, A. Frank. *Design of Control Systems*. Englewood Cliffs, NJ: Prentice-Hall, Inc, 1988.
- Donahue, Raymon A.; Poulson, Mary E.; and Edwards, Gerald E. 1997. "A method for measuring whole plant photosynthesis in *Arabidopsis thaliana*." *Photosynthesis Research* **52**: 263 – 269.
- Duffie, John A. and Beckman, William A. *Solar Engineering of Thermal Processes*. Hoboken, NJ: John Wiley and Sons, 2006.
- Eissenstat, D.M.; Graham, J.H.; Syvertsen, J.P.; and Drouillard, D.L. 1993. "Carbon Economy of Sour Orange in Relation to Mycorrhizal Colonization and Phosphorous Status." *Annals of Botany* **71**: 1 – 10.
- Heath, O.V.S. *The Physiological Aspects of Photosynthesis*. Stanford, CA: The Stanford University Press, 1969.
- Hines, Anthony L.; Ghosh, Tushar K.; Loyalka, Sudarshan K.; and Warder, Richard C. *Indoor Air Quality and Control*. Englewood Cliffs, NJ: PTR Prentice-Hall, Inc, 1993.
- "Interfacing Custom Chambers to the LI-6400 Sensor Head." *Application Note: LI-6400 Portable Photosynthesis System*. Vol 3. LI-COR, Inc.
- Lawlor, David W. *Photosynthesis*. 3<sup>rd</sup> ed. New York: Springer, 2001.
- Lawrence, Mark G. February 2005. "The Relationship between Relative Humidity and the Dewpoint Temperature in Moist Air: A Simple Conversion and Applications." *American Meteorological Society*.

- Mancini, Ron, Editor in Chief. *Op Amps for Everyone*. 2<sup>nd</sup> ed. Newnes, 2003.
- “Measuring Canopy Gas Exchange with the LI-6400 Portable Photosynthesis System.”  
*Application Note: LI-6400 Portable Photosynthesis System*. Vol 2. LI-COR, Inc.
- Miller, D.P.; Howell, G.S.; and Flore, J.A. 1996. “A Whole-plant, Open, Gas-exchange System for Measuring Net Photosynthesis of Potted Woody Plants.” *HortScience* **31(6)**: 944 – 946.
- Moran, Michael J. and Shapiro, Howard N. *Fundamentals of Engineering Thermodynamics*. 4<sup>th</sup> ed. Hoboken, NJ: John Wiley and Sons, 2000.
- Munson, Bruce R.; Young, Donald F.; and Okiishi, Theodore H. *Fundamentals of Fluid Mechanics*. 5<sup>th</sup> ed. Hoboken, NJ: John Wiley & Sons, Inc, 2006.
- Nobel, Park S. *Physiochemical and Environmental Plant Physiology*. San Diego, CA: Academic Press, Inc, 1991.
- Papanastasiou, Tasos C. *Applied Fluid Mechanics*. Englewood Cliffs, NJ: PTR Prentice Hall, 1994.
- Pearcy, R.W.; Ehleringer, J.; Mooney, H.A.; and Rundel, P.W., eds. *Plant Physiological Ecology: Field Methods and Instrumentation*. London: Chapman and Hall, 1994.
- Royer, Dana L.; Osborne, Colin P.; and Beerling, David J. 2005. “Contrasting seasonal patterns of carbon gain in evergreen and deciduous trees of ancient polar forests.” *Paleobiology* **31(1)**: 141 – 150.
- Sestak, Z.J.; Catsky, J.; and Jarvis, P.G., eds. *Plant Photosynthetic Production: Manual of Methods*. The Hague: Dr. W. Junk N.V. Publishers, 1971. p 571 – 572.
- “Using the LI-6400 Portable Photosynthesis System.” *Manual: LI-6400 Portable Photosynthesis System*. Version 5. LI-COR, Inc.
- White, Frank M. *Heat and Mass Transfer*. Reading, MA: Addison-Wesley Publishing Company, 1988.

## Appendix A: Fluid Flow Calculations

### Location one: top of entry pipe

P	1 atm
V	0 m/s
z	4 m

### Location two: exit after chamber

P	1 atm
V	2.12206591 m/s
z	0.1 m

**Table 15. Basic Bernoulli equation parameters**

Location	Diameter (m)	Area (m <sup>2</sup> )	Overall Length (m)
intake	0.06	0.0028274	4
general	0.02	0.0003142	0.5
H2O control	0.01	7.854E-05	0.2

**Table 16. Dimensions of pipe sections used in plumbing analysis**

Type	Number of fittings	Loss coefficient	Location	Velocity at fitting	Total loss term
45 degree joint	4	0.4	General	2.23	4.0
4:1 restriction	3	0.42	Humidity	8.91	50.0
1:4 expansion	3	0.5625	Humidity	8.91	67.0
Entrance	1	1	General	2.18	2.4
Exit	2	0.5	General	2.18	2.4
Valves	3	10	Humidity	8.91	1191.5

**Table 17. Minor losses calculations**

Section	Diameter (m)	Overall Length (m)	Velocity (m/s)	Reynolds number	Flow type	Friction factor	Total loss term (J/kg)
Intake	0.06	4	0.25	962	Laminar	0.067	0.14
General	0.02	0.5	2.23	2886	Neither (laminar)	0.022	1.38
Humidity control	0.01	0.2	8.91	5773	Turbulent	0.036	28.60

**Table 18. Major losses calculations**

Particle diameter (m)	0.002
Height of bed (m)	0.2
Area of bed (m <sup>2</sup> )	0.02
Porosity of bed	0.28
Superficial velocity	0.035

Total losses	139.962756
--------------	------------

**Table 19. Packed bed losses calculations**

Gains required (J/kg)	1451.372803
Power by blower (W)	1.197995237

Location	Pressure (Pa, gage)	Pressure (psi, gage)
Before one H2O ctrl valve	1688.622246	0.244913951
Entrance of flow meter	40.57240044	0.005884529

**Table 20. Results of Bernoulli analysis: blower power needed and pressures at points in flow**

## Appendix B: Dehumidifier Calculations

### Dehumidifier Calculations

Diameter	2 - 5	mm
Surface area	760	m <sup>2</sup> /g
Pore volume	0.43	cm <sup>3</sup> /g
Porosity	0.3096	
Bulk density	0.72	kg/L

**Table 21. Properties of silica gel. From ADCOA data sheet**

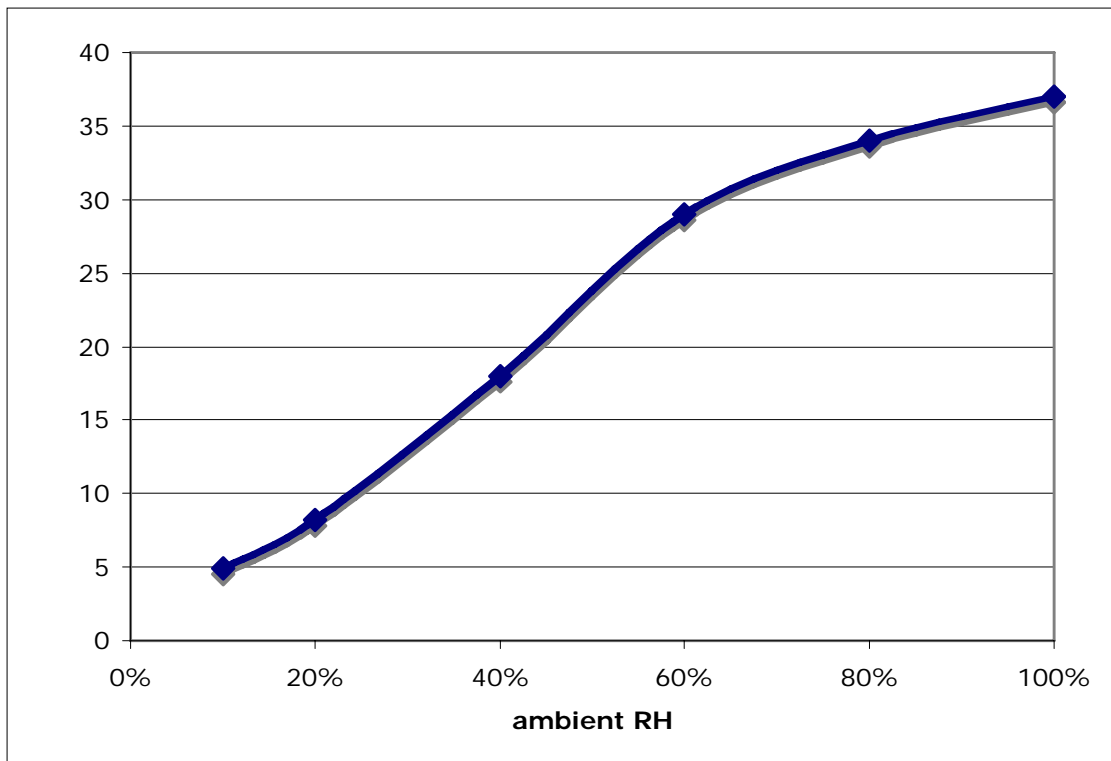


**Figure 23. Silica gel adsorption as varies with relative humidity**

Data from <http://www.ecompressedair.com/desiccant/silicagel.shtml>

Flow rate	11	gpm
	0.000693992	m <sup>3</sup> /s
Max density air (0 C, 1 atm)	1.292	kg/m <sup>3</sup>
Max mass flow rate	0.000896638	kg/s
	77.46951244	kg/day
Max absolute humidity (27 C)	25.96	g/m <sup>3</sup>
Max mass flow rate H2O	0.018016037	g/s
	1.55658556	kg/day
Min RH	0.3	x100 for %
Max H2O removed	1.089609892	kg/day
Adsorption	330	g/kg
<b>Silica gel needed</b>	1.650924078	kg/half day
	3.639664567	lb/half day
	<b>2.292950109</b>	<b>L/half day (12 hrs)</b>

**Table 22. Calculations of volume of silica gel needed. The adsorption of silica gel value is from Figure 10**

**Stoichiometric length (LUB-Equilibrium method)**

Concentration of H2O in influent	1.29606E-06	mol/cm <sup>3</sup>
Concentration of H2O in equilibrium with initial concentration of solute on adsorbent	1.29606E-07	mol/cm <sup>3</sup>
Initial concentration of H2O on silica gel	0.049	g/g
Saturation capacity of silica gel	0.37	g/g
Density of adsorbent	0.72	g/cm <sup>3</sup>
Molecular weight of adsorbate	20.03	g/mol
Time to breakthrough	43200	s
Superficial velocity	0.085600691	m/s
Length of stoichiometric wavefront	0.373827017	m
	14.71759908	in

**Table 23. Stoichiometric length calculations for 4" diameter pipe. A 4" diameter pipe requires an 11.13" height to hold 2.29 L, so the stoichiometric length is more than sufficient to hold the required volume of silica gel**

## Appendix C: Humidifier Calculations

Vapor pressure	3170	Pa
SA bubble	0.000314159	m <sup>2</sup>
Molar mass water	0.018016	kg/mol
Molar mass air	0.02897	kg/mol
R (gas constant)	8.314	J/mol-K
Temperature	298.15	K
V bubble	5.23599E-07	m <sup>3</sup>
Density air	1.168	kg/m <sup>3</sup>
Ambient pressure	101300	Pa

P	0.00107109
Q	89996.33227

**Table 24. Calculations to determine rate of water evaporating into bubbles. The P and Q are parameters in a differential equation developed in section **MEH****

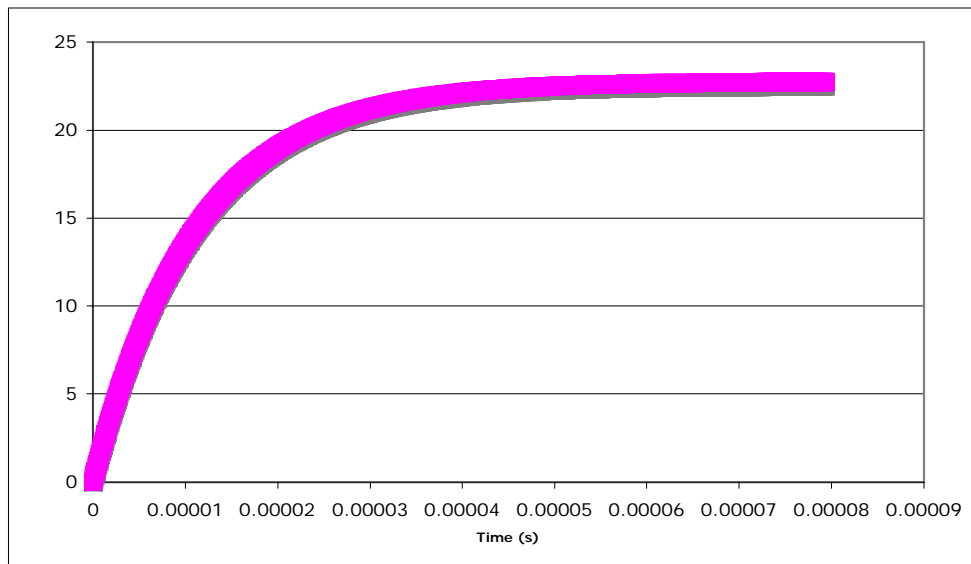


**Figure 24. Graph of water concentration in bubble versus time**

The asymptote the water is approaching represents 100% relative humidity. Since all bubbles will be saturated after less than a ten-thousandth of a second, the air leaving the humidifying column should be at 100% relative humidity for the temperature in the humidifier.

Daily flow rate of water required	0.466975668	kg/day
Volume H <sub>2</sub> O needed	0.466975668	L/day
	0.000466976	m <sup>3</sup> /day
Height bubbler	0.17	cm
Area bubbler	0.002746916	m <sup>2</sup>
Diam bubbler	5.913951037	cm

**Table 25. Volume of water required to humidify air from 0 to 30% relative humidity at 27 C**

**The daily flow rate required is from the calculations done for dehumidifying air from 100 to 70% relative humidity at 27 C. The dimensions correspond to a 3" diameter pipe 6.7" tall.**

## Appendix D: MatLab Energy Balance Code for TEC Sizing

```
% MASSIVE ENERGY BALANCE on chamber to size TECs

clear
clc

% Highly variable parameters

airTemp = 27; % Celsius
groundTemp = 30; % Celsius

chamberTemp = 20; % Celsius
flowRate = 11; % gallons per minute

% THE SUN
% Calculating the heat input from the sun is hard. We
% calculate the heat input during the hour 12 - 1 pm as probably the
time
% of day experiencing the most solar radiation. We estimate the hourly
% radiation from monthly daily averages, then find the amount of
radiation
% transmitted through all 5 sides of the chamber. We take into account
% the radiation transmitted through the other side to find the net
% radiation into the box. We'll divide by 3600 s to get the power input
% over the hour.

% Parameters of location and time
% These particular parameters are for an average day in San Juan, Puerto
% Rico in July between noon and 1 pm

latitude = 18.4 * pi / 180; % radians
avgDailyRad = 21.27*10^6; % Joules per meter squared
KBar_T = .55; % unitless
avgTemp = 27; % Celsius
delta = 21.2 * pi / 180; % radians
omega = 7.5 * pi / 180; % radians

reflectance = .3; % unitless

% Parameters of materials
% These particular parameters are for clear acrylic sheet
% The format of the arrays representing properties for all the sides at
% once is: [top, north, south, east, west].

tau = .9; % transmittance
base = 8; % inches, length of side of square base
height = 10; % inches, height of box
area = [base^2, base*height, base*height, base*height, base*height] *
0.00064516; % meters squared

beta = [0,90,90,90,90] * pi / 180; % radians
gamma = [0,180,0,-90,90] * pi / 180; % radians

% Calculate angle of incidence, R_b, etc
incidenceAngle = acos(sin(delta).*sin(latitude).*cos(beta) - ...
    sin(delta).*cos(latitude).*sin(beta).*cos(gamma) + ...
    cos(delta).*cos(latitude).*cos(beta).*cos(omega) + ...
    cos(delta).*sin(latitude).*sin(beta).*cos(gamma).*cos(omega) + ...
    cos(delta).*sin(beta).*sin(gamma).*sin(omega));
zenithAngle = acos(cos(latitude)*cos(delta)*cos(omega) +
sin(latitude)*sin(delta));
beamRatio = (cos(incidenceAngle) / cos(zenithAngle) +
abs(cos(incidenceAngle) / cos(zenithAngle)))/2; % R_b
```

```

betaA = beta * 180 / pi; % beta in angles
incidenceAngleDiffuse = (59.7 - .1388*betaA + .001497*betaA.^2) * pi /
180; % incidence angle of diffuse radiation, eqn 5.4.2
incidenceAngleReflected = (90 - .5788*betaA + .002693*(betaA.^2)) * pi /
180; % incidence angle of reflected radiation, eqn 5.4.1

sunsetAngle = acos(-tan(latitude)*tan(delta));

% Convert monthly daily average radiation to hourly beam and diffuse
radation
if sunsetAngle > 81.4 * pi / 180
    HBardOverHBar = 1.311 - 3.022 * KBar_T + 3.427 * KBar_T^2 - 1.821 *
KBar_T^3;
else
    HBardOverHBar = 1.391 - 3.560 * KBar_T + 4.189 * KBar_T^2 - 2.137 *
KBar_T^3;
end

avgDailyDiff = HBardOverHBar * avgDailyRad; % diff stands for diffuse
avgHourlyDiff_over_avgDailyDiff = pi/24 * (cos(omega) -
cos(sunsetAngle)) / (sin(sunsetAngle) - sunsetAngle*cos(sunsetAngle)); %
eqn 2.13.4
avgHourlyDiff = avgHourlyDiff_over_avgDailyDiff * avgDailyDiff;

sunsetAngleA = sunsetAngle * 180/pi;
a = .409 + .5016*sind(sunsetAngleA - 60);
b = .6609 - .4767*sind(sunsetAngleA - 60);
avgHourly_over_avgDaily = pi/24 * (a + b*cos(omega)) * (cos(omega) -
cos(sunsetAngle)) / (sin(sunsetAngle) - sunsetAngle*cos(sunsetAngle)); %
eqn 2.13.2a
avgHourly = avgHourly_over_avgDaily * avgDailyRad;
avgHourlyBeam = avgHourly - avgHourlyDiff;

% Calculate net radiation transmitted through sides
transBeamRad = avgHourlyBeam * beamRatio * tau;
transDiffRad = avgHourlyDiff * tau * (1 + cos(beta))/2;
transReflRad = reflectance * avgHourly * tau * (1 - cos(beta))/2;

transRad = [transBeamRad; transDiffRad; transReflRad];
S = sum(transRad); % J/m^s

% subtract radiation passing through to other side
% calculate percent radiation hitting a wall
incAngles = [incidenceAngle; incidenceAngleDiffuse;
incidenceAngleReflected];

for i = 1:3,
    for j = 2:5
        if abs(tan(incAngles(i,j))) < height/base
            fracTransmit(i,j) = (height -
base*tan(incAngles(i,j)))/height;
        else
            fracTransmit(i,j) = 0;
        end
    end

    if abs(tan(incAngles(i,1))) > base / height
        fracTransmit(i,1) = (base/tan(incAngles(i,1)))/height;
    else
        fracTransmit(i,1) = 0;
    end
end
end

```

```

% subtract out losses from radiation input
lostRad = transRad.*fracTransmit*tau;
actualTransRad = transRad - lostRad;
actualInputRadiation = sum(actualTransRad);

% Finally calculate net energy input from solar radiation
energyEntering = actualInputRadiation.*area; % Joules
powerEntering = energyEntering / 3600; % Watts
totalSunPower = sum(powerEntering) % Watts

% THE AIR
% We're assuming the temperature on the inside edge of the box is the
same
% as the average temperature inside the box, because we're mixing up the
% air with a fan. We're currently modeling forced and free convection
along a flat
% plate, laminar flow. I'm assuming for forced convection, a flat plate
is
% horizontal or vertical. I'm also assuming that the wind speed is the
% same on every face.

% Parameters of properties of acrylic (should include Teflon too)
thermalCondAcr = .186; % W/m-K, from
http://www.arco.cz/catalog/OpticalFilters.pdf
thicknessAcrChamb = .25 * .0254; % meters, .25 in and .0254 for
conversion
condHeatTransCoeffAir = thermalCondAcr / thicknessAcrChamb; % W/m^2-K

% Forced convection at surface of box

windVelocity = 20; % m/s, outside wind speed, higher is more
conservative
kVisc = 0.000016136335; % m^2/s kinematic viscosity of air at 27 C, from
http://users.wpi.edu/~ierardi/FireTools/air_prop.html
thermDiff = 0.0000239967199999999998; % m^2/s thermal diffusivity air,
from above
thermCond = 0.026197599; % W/mK thermal conductivity of air, from above
lengthForced = base * .0254 * ones(1,5); % the characteristic length,
the length of the plate along which wind is blowing

reynolds = windVelocity .* lengthForced / kVisc; % Reynolds number
checkTurbForced = 500000 - reynolds % transition to turbulent at 500000
for flat plate, White p 324
prandtl = kVisc / thermDiff; % Prandtl number

nusseltForced = .664 * reynolds.^(1/2) * prandtl^(1/3); % from White,
Heat and Mass Transfer, p 294

% Free convection at surface of box
g = 9.81; % gravitational constant
tAvg = (chamberTemp + airTemp)/2;
tDiff = abs(chamberTemp - airTemp);
coeffThermExp = 1/tAvg;
lengthFree = [base, height, height, height, height] * .0254;

grashof = g * coeffThermExp * tDiff * lengthFree.^3 / kVisc^2; % if were
correct, would change kVisc to value for tAvg
rayleigh = grashof * prandtl;
checkTurbFree = 10^9 - grashof

nusseltFree = (8/3)*prandtl^(1/2)*grashof.^(1/4)/(336*(prandtl +
5/9)).^(1/4); % White p 395
nusseltFree(1) = .54*rayleigh(1)^(1/4); % White p 405

```

```

% Combining free and forced convection
% Assumes worst case: free and forced help each other

for i = 1:length(grashof)
    qual = grashof(i) / reynolds(i)^2; % White, p 414
    if qual < 100 & qual > .01 % neither dominates
        nusseltOverall = (nusseltForced(i)^3 + nusseltFree(i)^3)^(1/3);
% White, p 415
        convHeatTransCoeffAir = nusseltOverall * thermCond /
lengthForced(i); % shorter length for conservative analysis
    elseif qual > 100 % free dominates
        convHeatTransCoeffAir = nusseltFree(i) * thermCond /
lengthFree(i);
    else % forced dominates
        convHeatTransCoeffAir = nusseltForced(i) * thermCond /
lengthForced(i);
    end
end

% Wrapping it up

heatTransCoeffAir = 1./(1./condHeatTransCoeffAir +
1./convHeatTransCoeffAir);

airHeatLoss = area .* heatTransCoeffAir * (airTemp - chamberTemp);

totalAirPower = sum(airHeatLoss)

% THE GROUND, all conduction

thicknessAcrGround = (3/8) * .0254; % meters
groundHeatTransCoeff = thermalCondAcr / thicknessAcrGround; % W/m^2-K
groundArea = base*base * 0.00064516; % meters^2, need .0006 for
conversion
totalGroundPower = groundArea * groundHeatTransCoeff * (groundTemp -
chamberTemp)

% control volume energy analysis putting the whole shebang together

% relevant parameters

enthalpyIn = 300190; % J/kg, from table A-22 in the library thermo book
enthalpyOut = (290.16 + (295.17 - 290.16)/(295 - 290) * (293 - 290)) *
1000;

areaIn = pi*(.05 / 2)^2; % m^2
areaOut = pi*(.05 / 2)^2;

densityAir = 1.2; % kg/m^3

massFlowRate = flowRate * 6.30901967*(10^-5) * densityAir; % kg/s, with
conversion 1 gpm = 6.306e-5 m^3/s

velocityIn = massFlowRate / (areaIn * densityAir); % m/s
velocityOut = massFlowRate / (areaOut * densityAir);

heightIn = .05; % m
heightOut = .25;

fanWatts = 2; % W, for work energy input to system

% This equation uses a control volume analysis and is a rearrangement of

```

```
% 0 = Q_dot - W_dot + m_dot_in*(h_in + V_in^2/2 + gz_in) -  
m_dot_out*(h_out + V_out^2/2 + gz_out)  
  
envHeatIn = totalSunPower + totalAirPower + totalGroundPower;  
workIn = fanWatts;  
  
flowHeatIn = massFlowRate * (enthalpyIn + (velocityIn^2)/2 +  
g*heightIn);  
flowHeatOut = massFlowRate * (enthalpyOut + (velocityOut^2)/2 +  
g*heightOut);  
  
inputCoolingPower = envHeatIn + workIn + flowHeatIn - flowHeatOut
```

## Appendix E. LI-6400 Files (Config file and ComputeList)

### Config File (edited to allow interface with analog input pins)

```
ComputeList= "OurComputeList"  
UserChan= 20 5 1  
UserChan= 21 6 1  
UserChan= 22 6 1  
UserChan= 23 5 1  
Displays= "StdDisplay_6.0"  
LogFormat= "StdLogFmt_6.0"
```

### Compute List

```
/* boundary layer */  
##10 "fda" "flow / area with units conversion"  
" (flow_um * 1E-6) / (area_cm2 * 1E-4) "  
  
##111 "BLC_1" "One sided BLC"  
" area_cm2 * blcSlope + blcOffset "  
  
##11 "BLCond" "Effective BLC"  
" #111 * (stom_rat + 1) * (stom_rat + 1) / (stom_rat * stom_rat + 1)"  
  
/* transpiration */  
##20 "Trans" "Transpiration (mol/m2/s)"  
" (h2o_2_mm - h2o_1_mm) / (1000.0 - h2o_2_mm) * #10"  
  
##21 "Trmmol" "Transpiration (mmol/m2/s)"  
" #20 * 1E3"  
  
/* energy balance deltaT */  
##2213F1 "Tair_K" "air temp in K"  
" tLeaf_c + 273.15"  
##2214F1 "Twall_K" "Twall temp K"  
" tCham_c + 273.15"  
##2216 "R(W/m2)" "incoming radiation"  
" (parIn_um * f_parIn + parOut_um * f_parOut) * alphaK "  
  
##2218 "Tl-Ta" "energy balance delta t"  
" (#2216 + 1.0773E-7 * ((#2214 ^ 4) - (#2213 ^ 4)) - #20 *  
44100.0) / (#111 * 56.0 + 4.3092E-7 * (#2213 ^ 4)) "  
  
/* leaf temp */  
##221F2 "CTleaf" "Computed leaf temp"  
" Tleaf_c + #2218 * doEB"  
  
/* leaf conductance */  
##222 "SVTleaf" "SatVap(Tleaf)"  
" ( 0.61365 * EXP(17.502 * #221 / (240.97 + #221))) "  
  
##223 "h2o_i" "intercellular h2o"  
" #222 * 1000 / press_kPa "  
  
##224 "h2odiff" "diff"  
" #223 - h2o_2_mm"  
  
##225 "CTair" "Computed chamber air temp"  
" $ doEB IF Tleaf_c ELSE Tcham_c Tleaf_c + 2 / THEN "  
  
##226 "SVTair" "SatVap(Tair)"
```

```

" ( 0.61365 * EXP(17.502 * #225 / (240.97 + #225))) "

##22 "CndTotal" "Total conductance"
" $ #224 0 <> IF 1000 #223 h2o_2_mm + 2 / - #224 / #20 * ELSE 0 THEN "

##23 "Cond" "Stomatal cond. (mol/m2/s)"
" $ #22 0 <> IF 1.0 1.0 #22 / 1.0 #11 / - / ELSE 0 THEN "

##24 "vp_kPa" "vapor pressure chamber air"
" h2o_2_mm * press_kPa / 1000 "

##25 "VpdL" "Leaf VPD (SatVap(Tleaf) - eair)"
" #222 - #24"

##27 "VpdA" "Air VPD (SatVap(tair) - eair)"
" #226 - #24"

/* photosynthesis */
##30 "Photo" "Photosynthesis (æmol/m2/s)"
" (co2_1_um - co2_2_um * (1000 - h2o_1_mm) / (1000 - h2o_2_mm)) * #10 "

##35 "CndCO2" "Total Conductance to CO2"
" 1.0 / (1.6 / #23 + 1.37 / #11)"

##36 "Ci" "Intercellular CO2 (æmol/mol)"
" ((#35 - #20/2) * co2_2_um - #30) / (#35 + #20/2)"

##38 "Ci_Pa" "Intercellular CO2 (Pa)"
" #36 * press_kPa * 1E-3"

##39 "Ci/Ca" "Intercellular CO2 / Ambient CO2"
" #36 / co2_2_um "

/* ball berry */
##51 "RHsfc" "Surface Humidity (%)"
" (1.0 - (#20 * press_kpa)/#222/#23) * 100"

##52 "C2Sfc" "Surface CO2 (æmol/mol)"
" co2_2_um - #30 / (#11 / 1.35)"

##53 "AHs/Cs" "Ball-Berry parameter "
" #30 * #51 /100.0 / #52 "

##61 "FRate" "Measured Flow Rate"
"chan20_mv"

##62 "CHumid" "Chamber Humidity"
"(chan21_mv -300) * 50/35"

##63 "InHumid" "Incoming Humidity"
"(chan22_mv - 300) 50 / 35"

##64 "InT" "Incoming Temperature"
"chan23_mv"

##66 "BubF" "Bubbler Flow"
"NOASSIGN
IF (#62 < 1.5E3)
AOSSET(5E3, 17)
ELSE
IF (#62 < 2E3)
AOSSET(2E4 - #62*10, 17)
ELSE
AOSSET(0, 17)

```

```
THEN  
THEN"
```

```
##67 "DessF" "Dessicator Flow"  
"NOASSIGN  
IF (#62 > 3.5E3)  
AASET(3.5E4 - #62*10, 18)  
ELSE  
IF (#62 > 3E3)  
AASET(5E3, 18)  
ELSE  
AASET(0, 18)  
THEN  
THEN"
```

```
##68 "NoFilterF" "No-Filter Flow"  
"NOASSIGN  
IF (1.5E3 < #62 < 2E3)  
AASET(#62*10 - 1.5E4, 19)  
ELSE  
IF (2E3 < #62 < 3E3)  
AASET(5E3, 19)  
ELSE  
IF (3E3 < #62 < 3.5E3)  
AASET(3.5E4 - #62*10, 19)  
ELSE  
AASET(0, 17)  
THEN  
THEN  
THEN"
```

## Appendix F: Additional Test Results

### Calibration of Volumetric Flow Meter

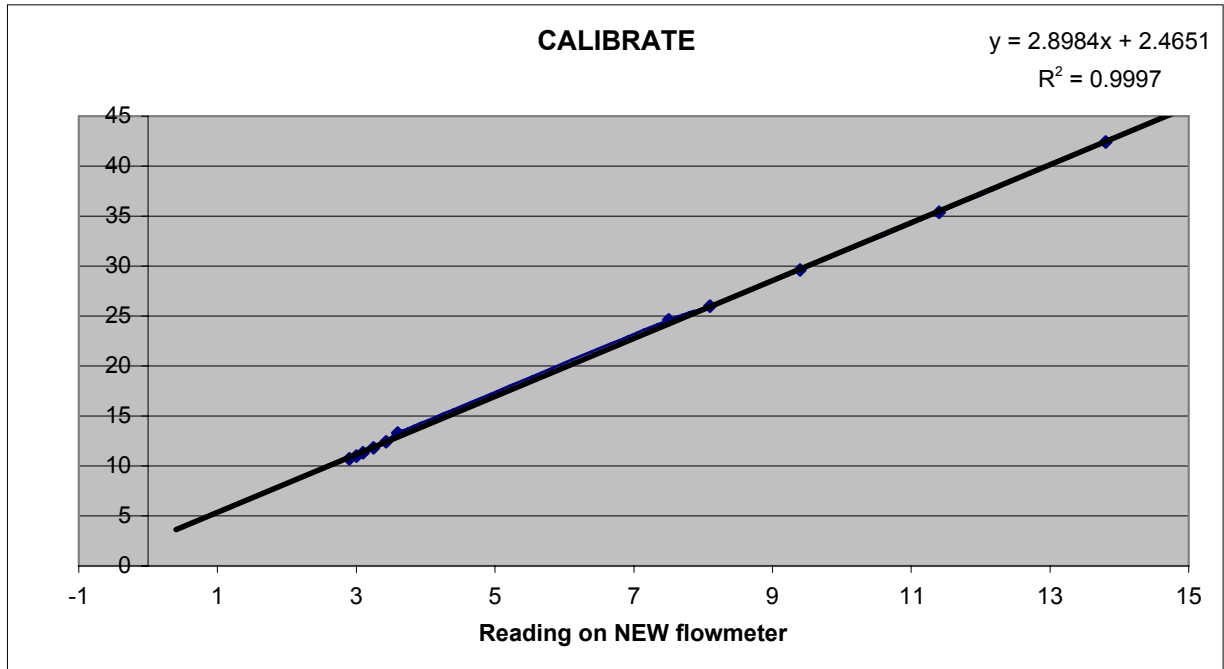


Figure 1. Another calibration curve for the rotameter. This earlier curve is assumed less accurate due to the experience gained during it.

### System Curve Test Results

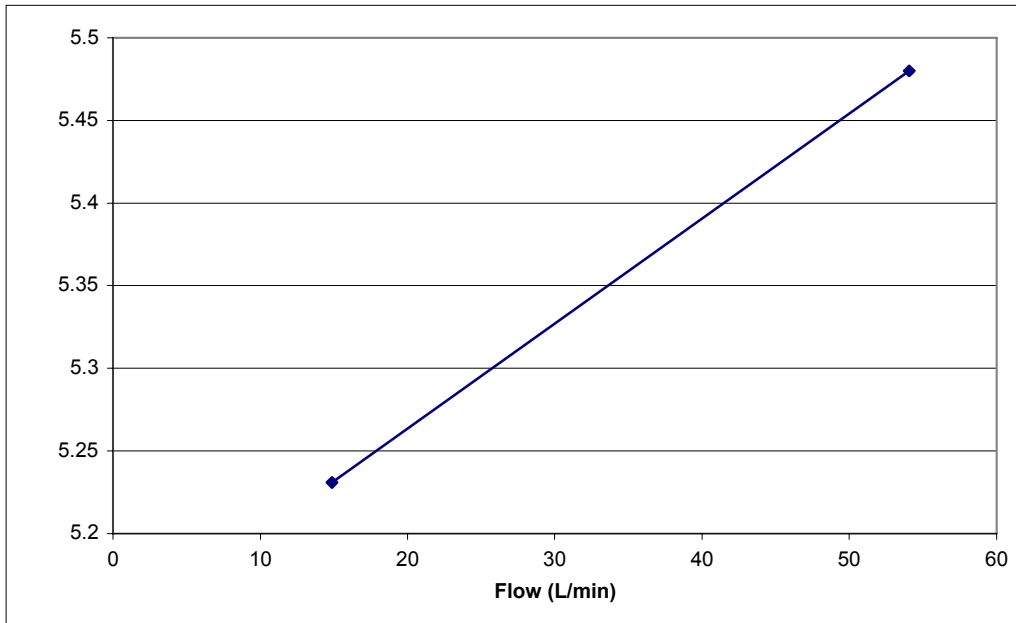


Figure 2. Volumetric flow meter. Intermediate results were not possible, but very little variation in pressure drop was observed.

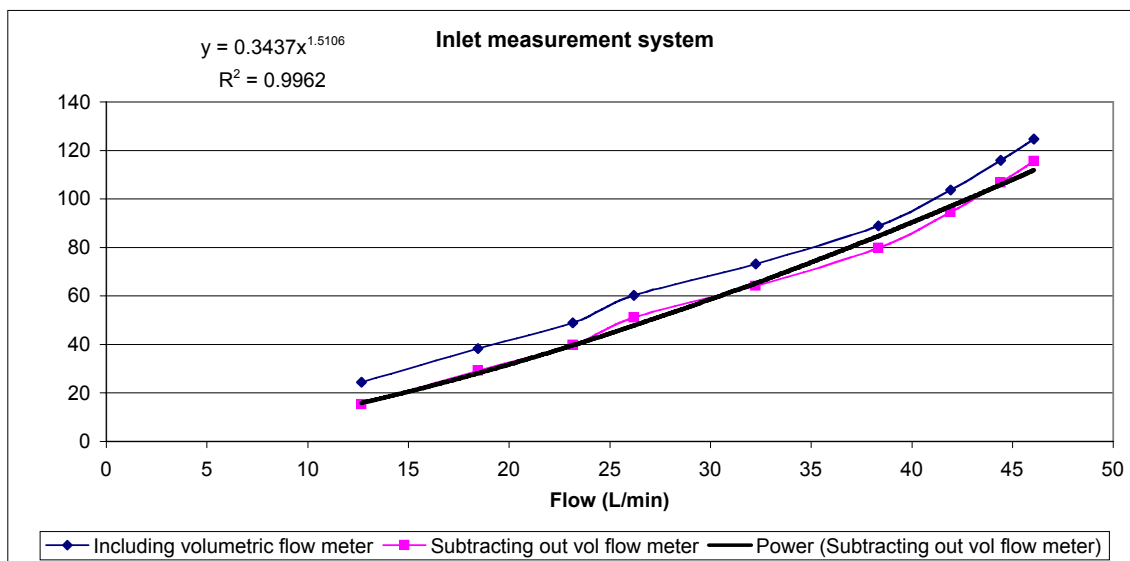


Figure 3. Inlet measurement system curve. Fitted curve:  $P = 0.3437F^{1.5106}$ , where P is pressure in mBar and F is flow in L/min.

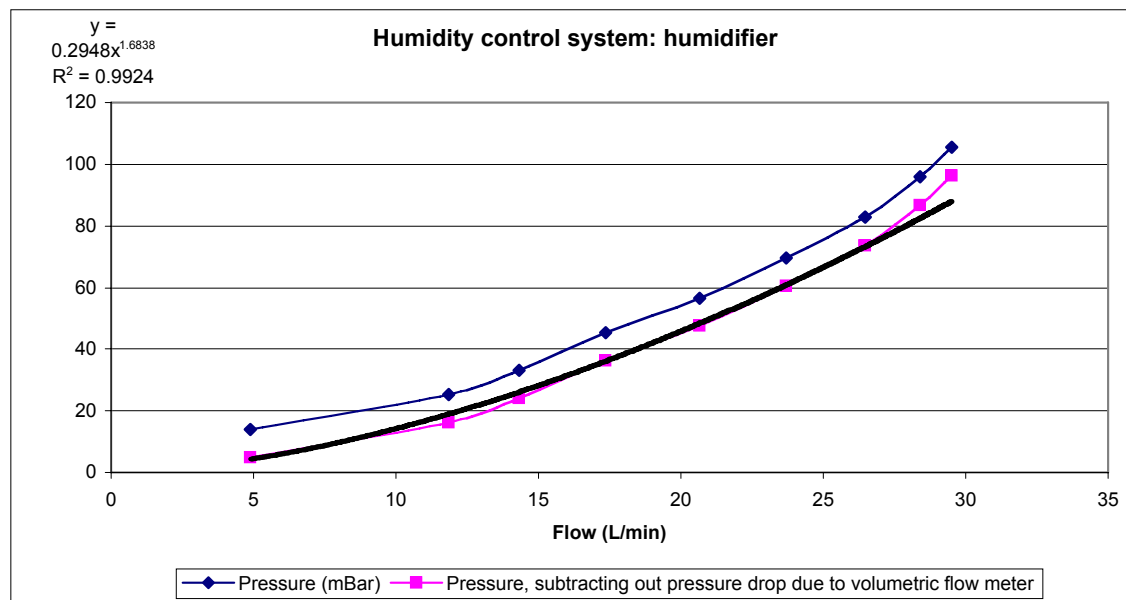


Figure 4. Humidifier system curve. Fitted curve:  $P = 0.2948F^{1.6838}$ , where P is pressure in mBar and F is flow in L/min.

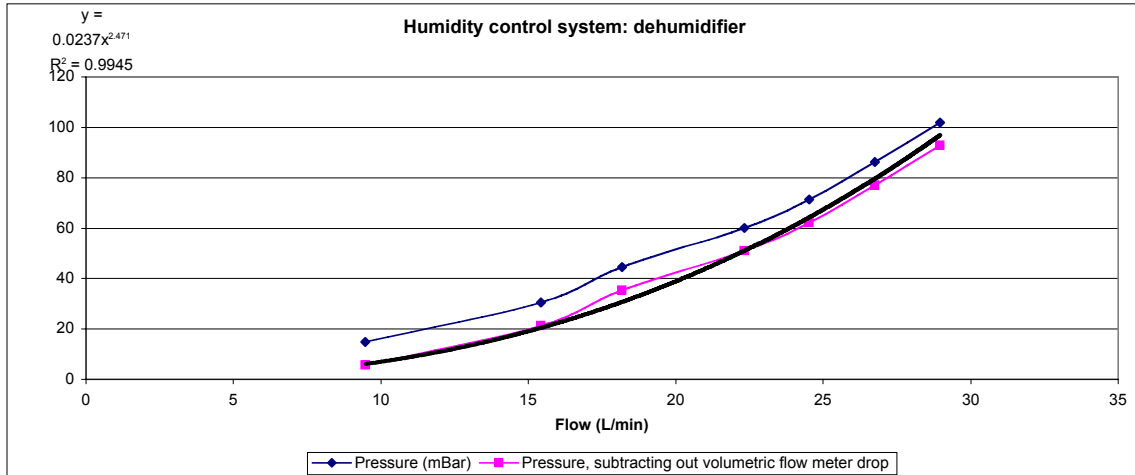


Figure 5. Dehumidifier system curve. Fitted curve:  $P = 0.0237F^{2.471}$ , where P is pressure in mBar and F is flow in L/min.

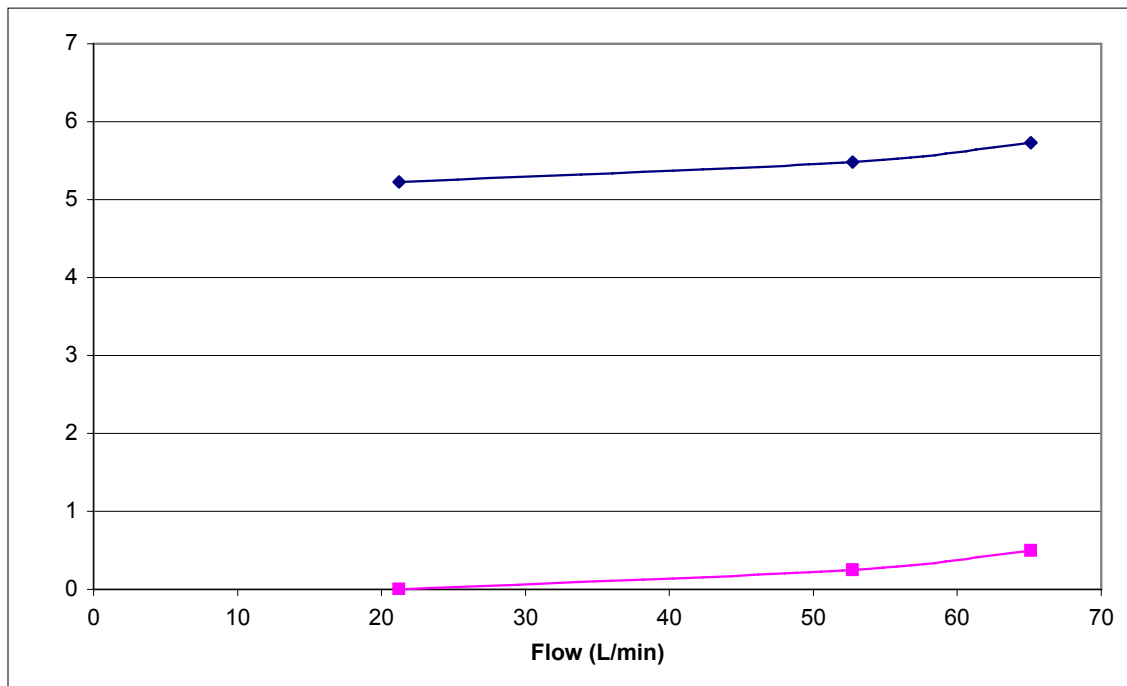


Figure 6. Measurement chamber system curve. The pressure drop across the chamber was so low it was assumed to be negligible in the overall system curve.

### Mixing Test Results

1: steady 3, fans on	plant	12
	inlet	9.4
	outlet	6.7
	q. sensor	7.3
2: steady	plant	19.8

3, fans on	inlet	16.3
	outlet	12.7
	q. sensor	12.8
3: 5 mins, fans on	plant	33.7
	inlet	29.2
	outlet	24.6
	q. sensor	24.4
4: 5 mins, fans off	plant	37.6
	inlet	34.9
	outlet	31.6
	q. sensor	26.9
5: 5 mins, fans off	plant	37.5
	inlet	34.2
	outlet	31.6
	q. sensor	27
6: 5 mins, fans on	plant	39.3
	inlet	32.4
	outlet	25.2
	q. sensor	25.5
7: 5 mins, fans on 13V	plant	31.3
	inlet	27.4
	outlet	23
	q. sensor	22.6
8: 5 mins, fans on 14V	plant	29.8
	inlet	25.1
	outlet	20.4
	q. sensor	20
9: 5 mins, fans on 15V	plant	31.9
	inlet	26.6
	outlet	21.1
	q. sensor	21.1

Table 1. Tabulated data from initial test. In this test, a hairdryer was placed at the blower and the blower ran at 12 V, resulting in a much larger flow rate than design. Tests 1 and 2 were disregarded because the temperature had clearly not reached steady state.

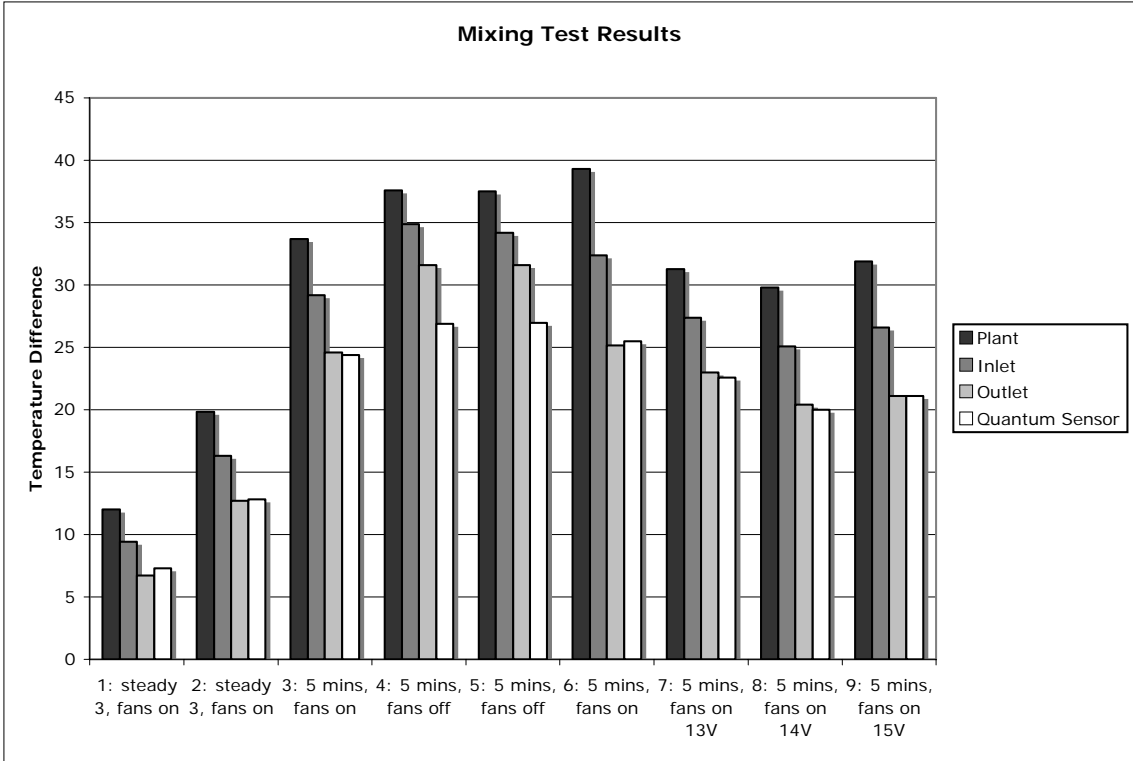


Figure 7. Graphical mixing test results from Table 1. In this test, mixing was noticeably poor. In addition, the fans served only to mix air between the outlet and the quantum sensor.

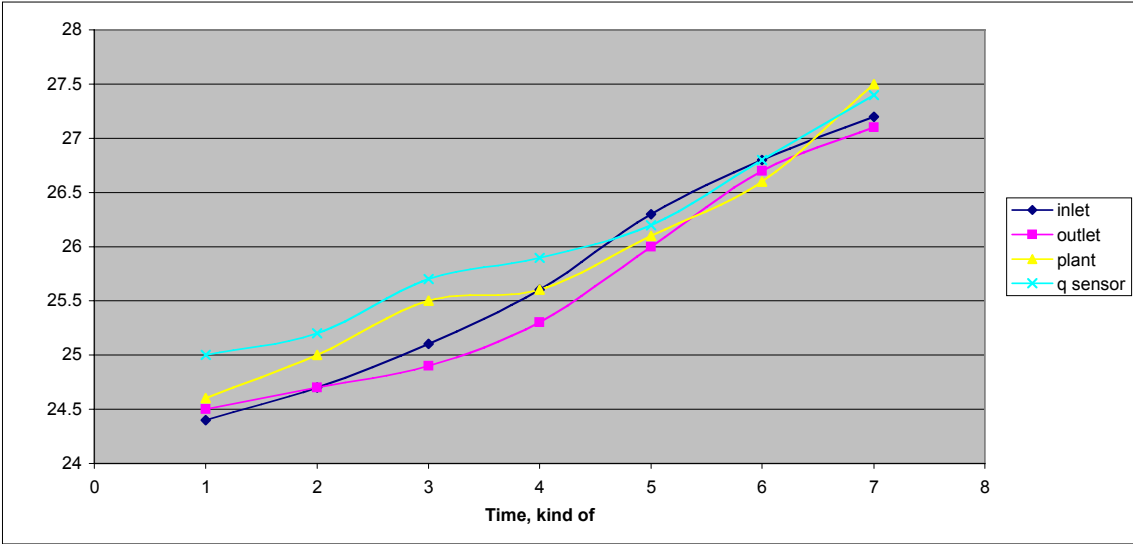


Figure 8. Mixing test results. In this test, a hairdryer at the blower inlet was again used, but the flow rate through the system was actually 42 L/min (as in all subsequent mixing tests). Mixing in this test is notably better than the previous tests.

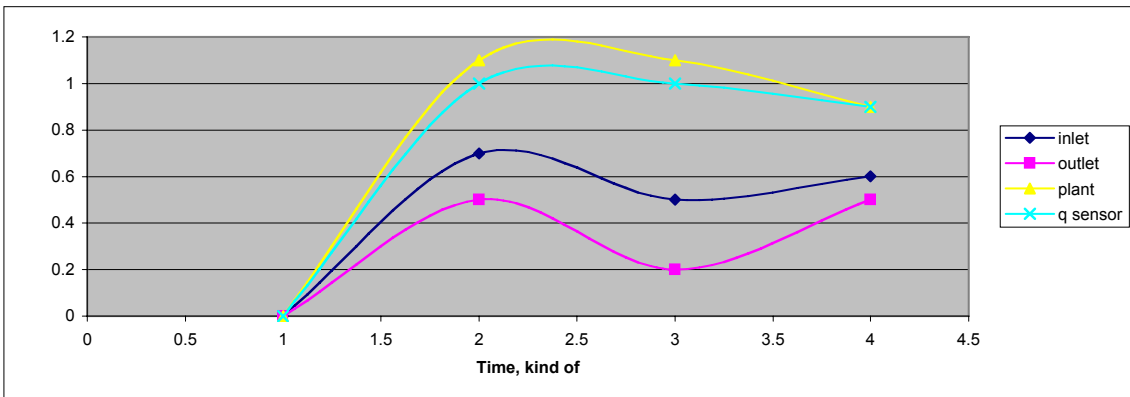
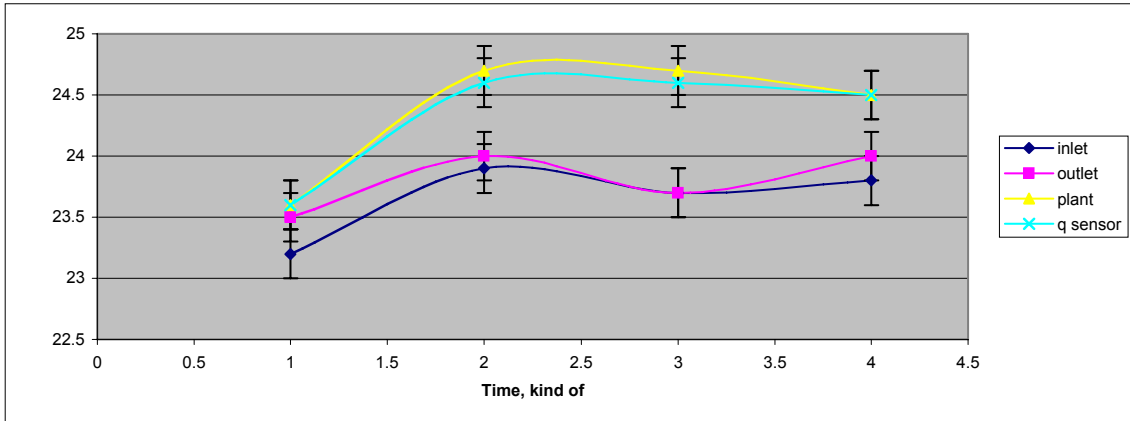
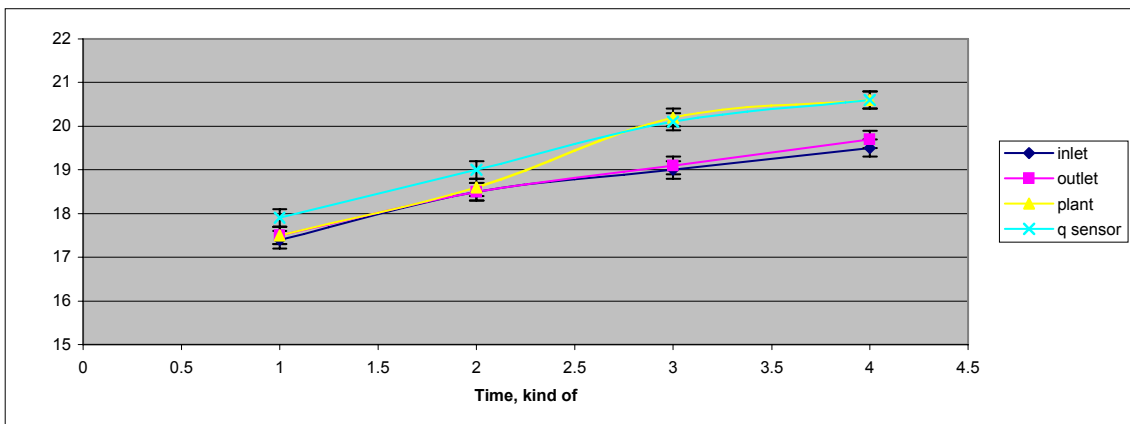


Figure 9. Mixing test results. In this test, the 5V voltage regulator at plant level was used with 6V across it. In this test, the plant and quantum sensor have similar temperatures, as do the inlet and outlet.



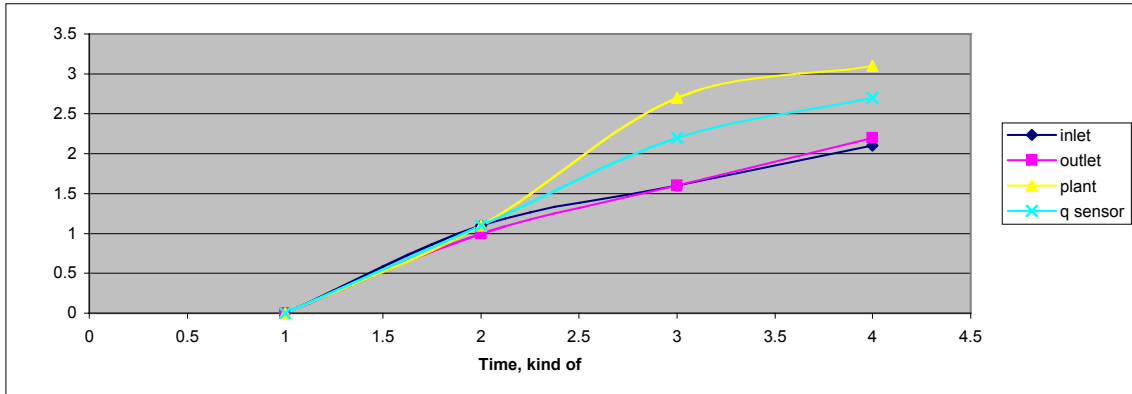


Figure 10. Mixing test results. In this test, the 5V voltage regulator at plant level was used with 9V across it. The pairing between the plant and quantum sensor, in addition to inlet and outlet is again visible.

### Temperature Control System Tests

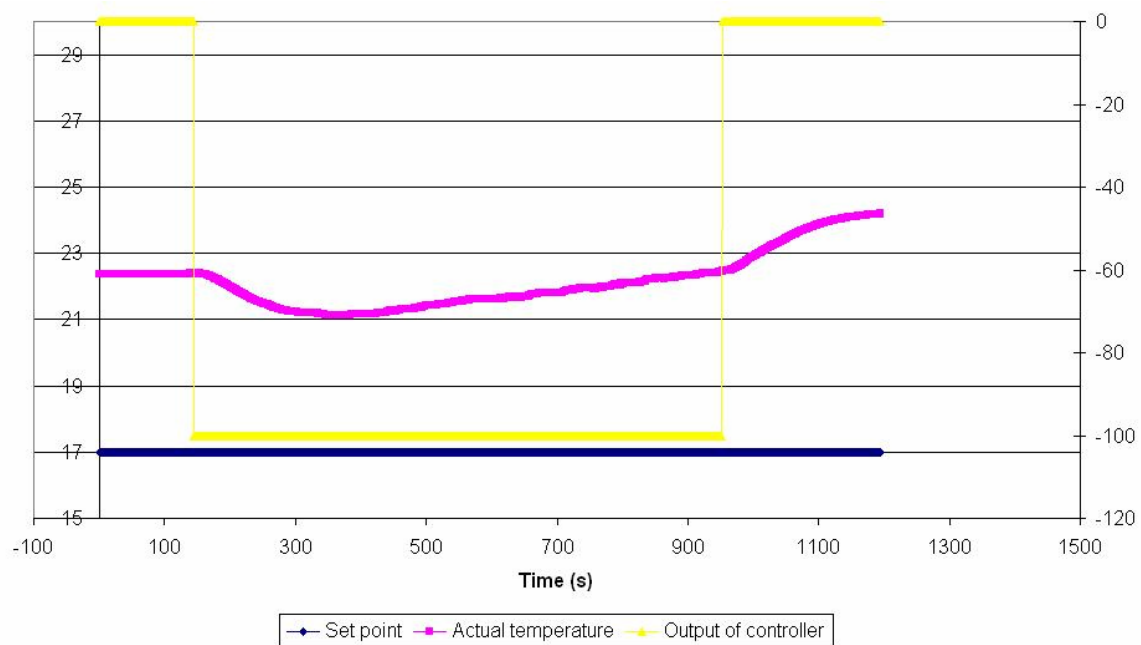


Figure 11. Test of temperature control system using additional fan blowing across ice.

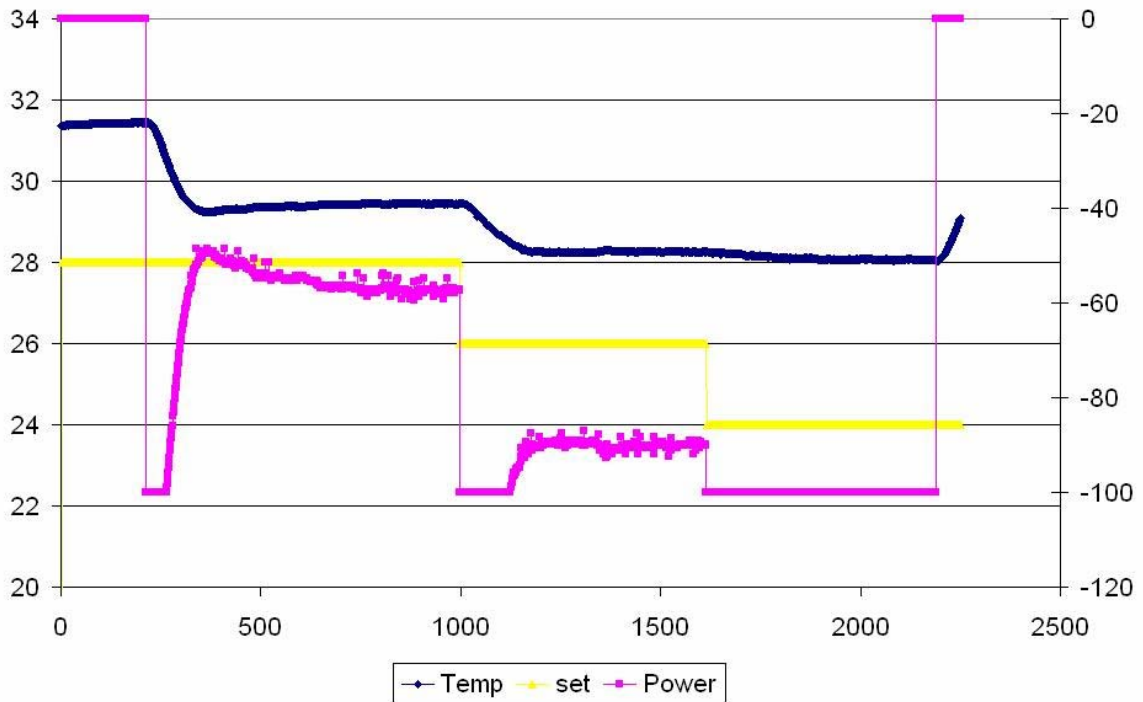


Figure 12. Test of temperature control system using additional layer of mylar.

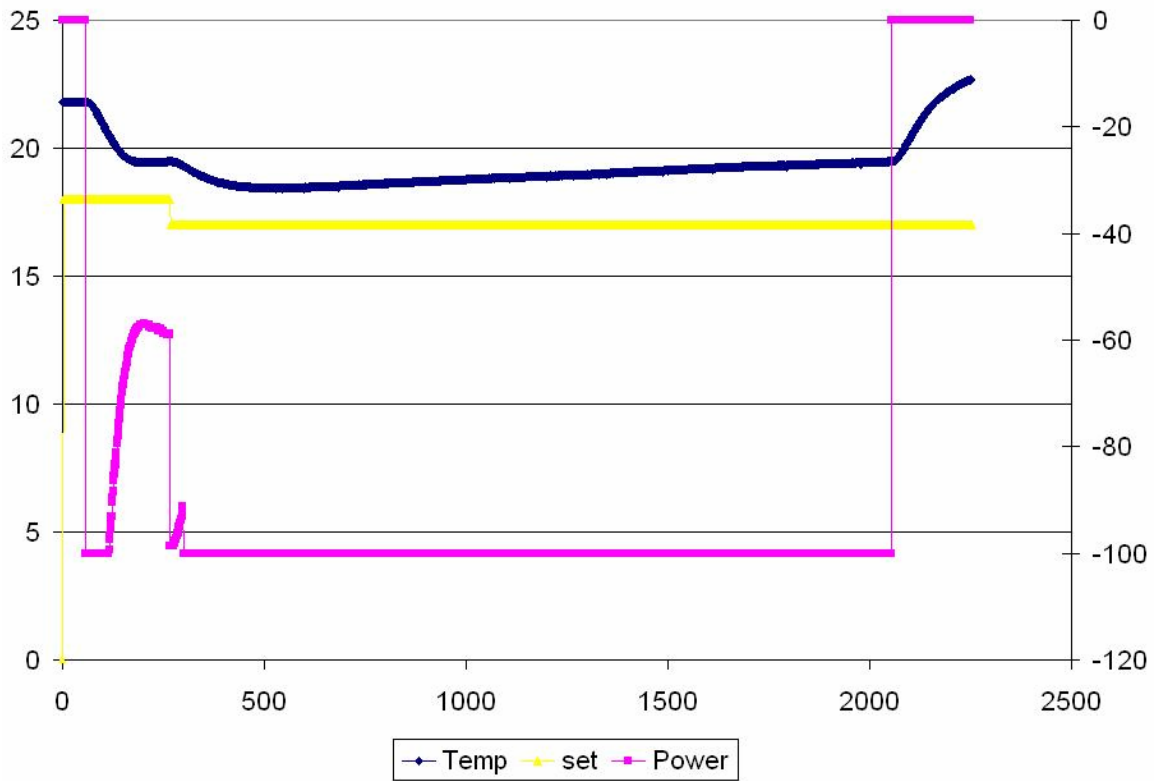


Figure 13. Test of temperature control system using complete mylar insulation around entire frame.

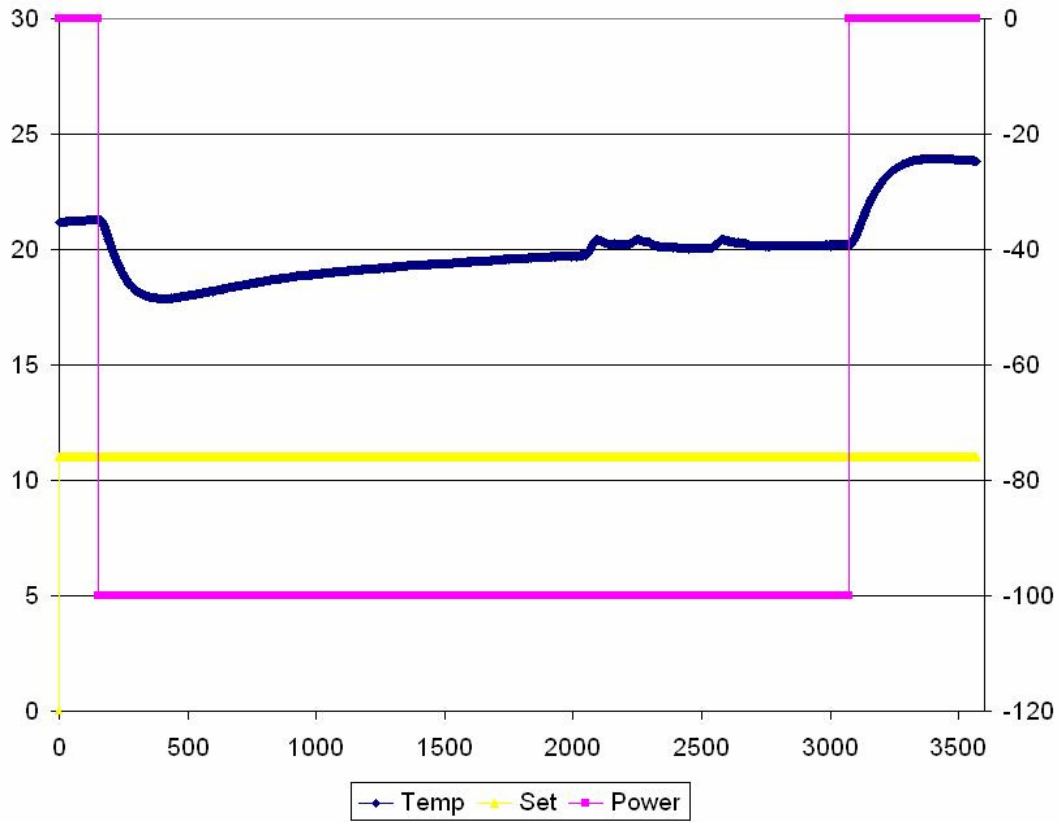


Figure 14. Test of temperature control system using internal heat sink fan.

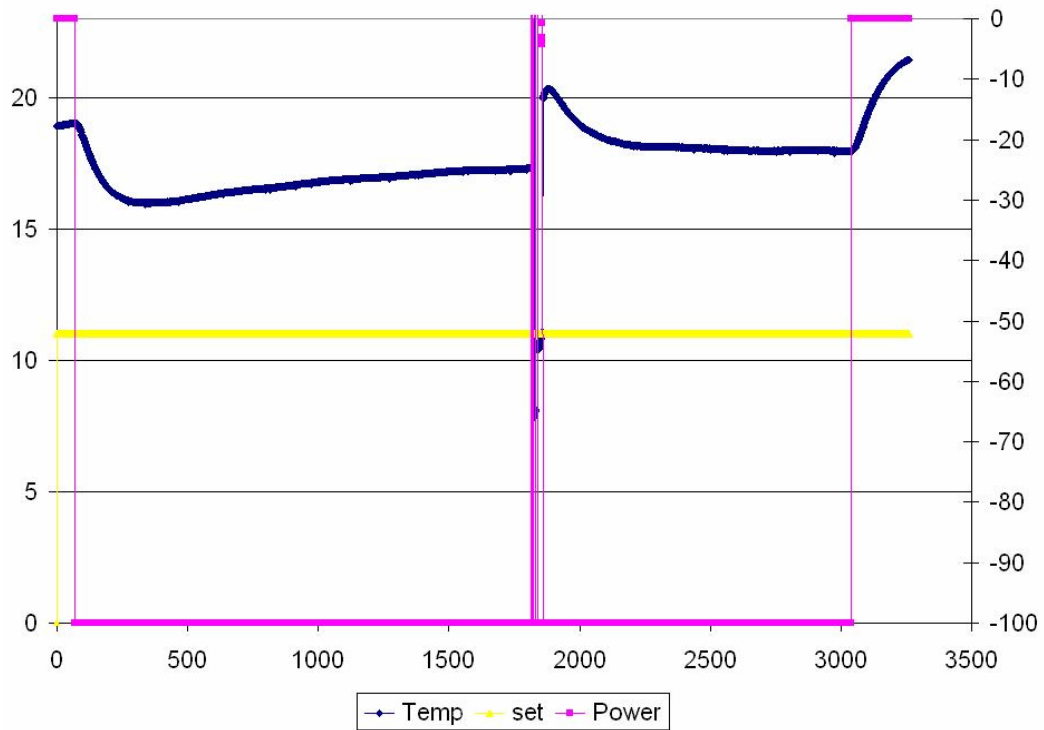


Figure 15. Second test of temperature control system using internal heat sink fan.

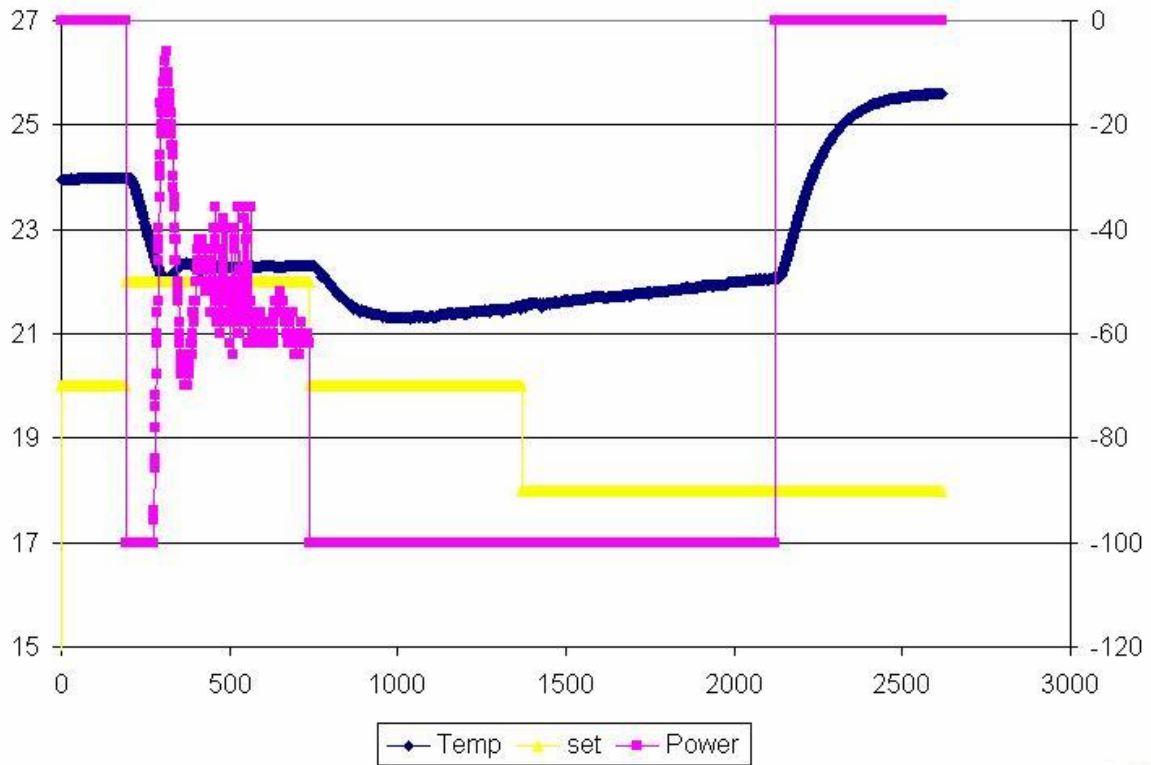


Figure 16. Test of temperature control system using bandwidth = 1.

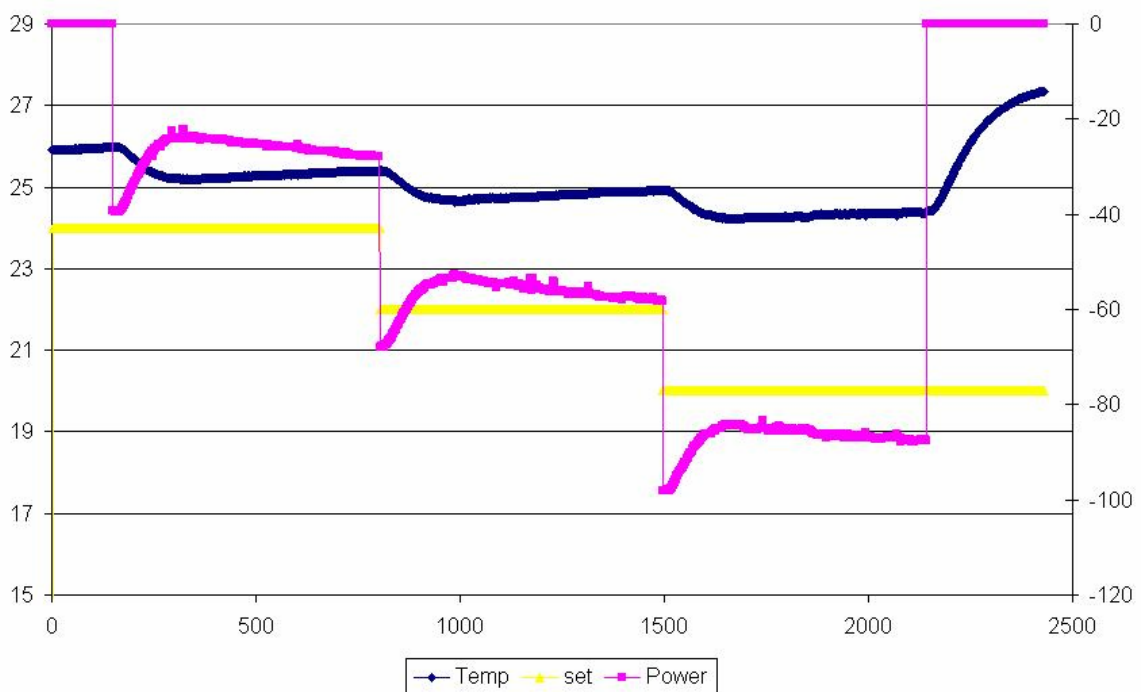


Figure 17. Test of temperature control system using bandwidth = 10.

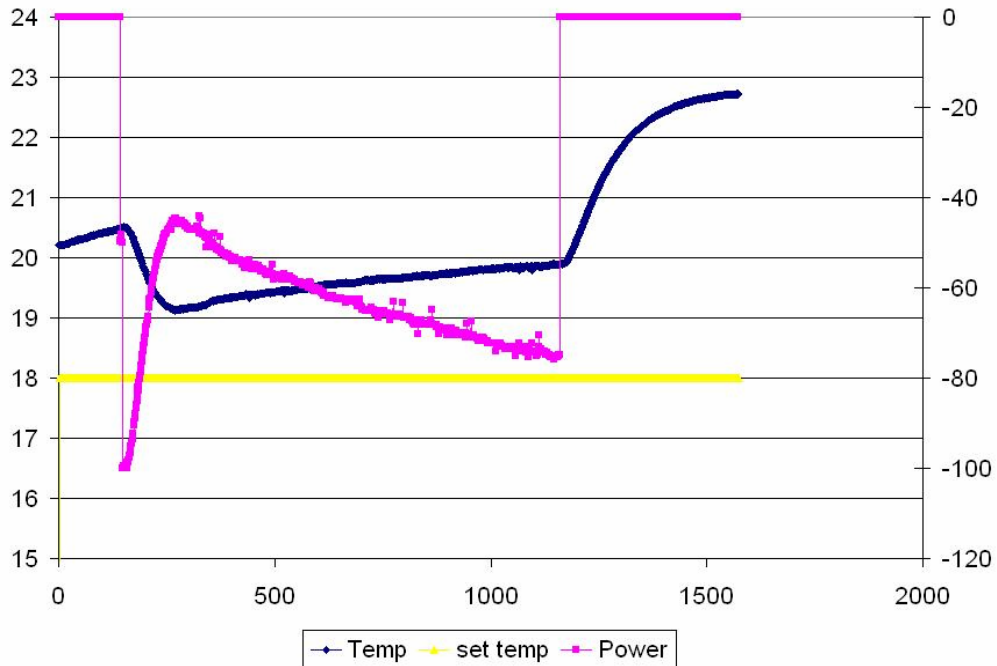


Figure 18. Test of temperature control system using a set point only 2 degrees below the initial temperature.

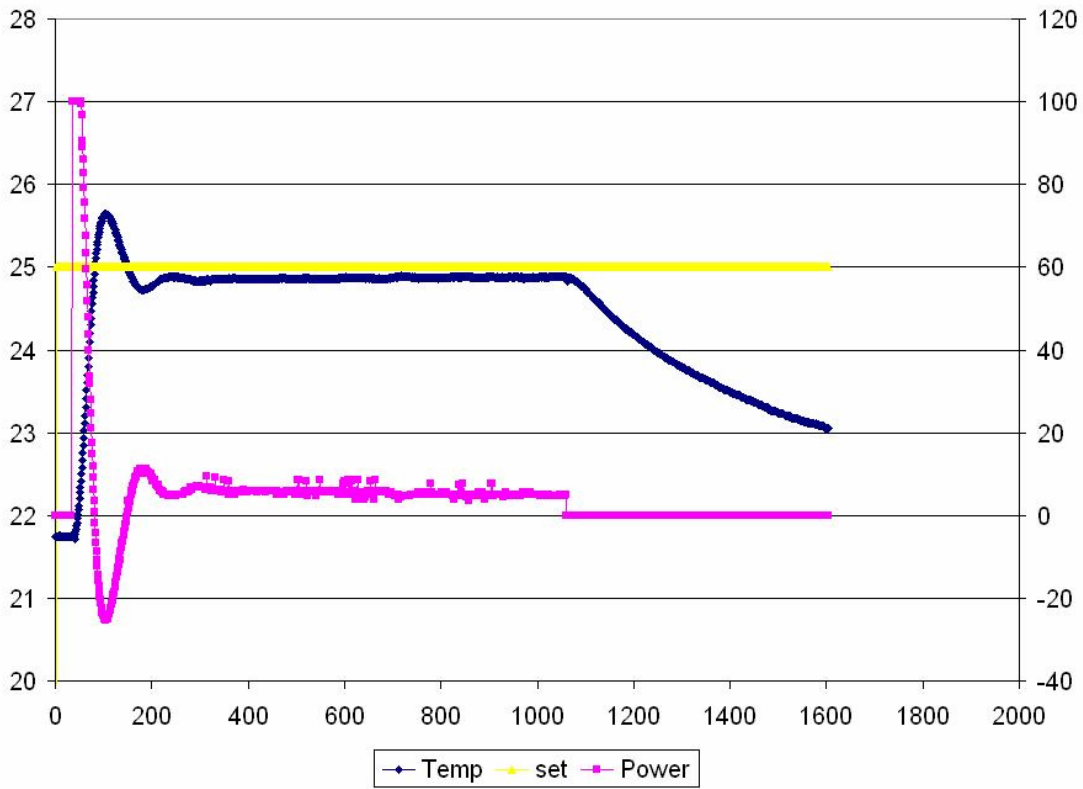


Figure 19. Test of temperature control system using hotter than ambient set point. Note that the temperature stabilized at the set point.

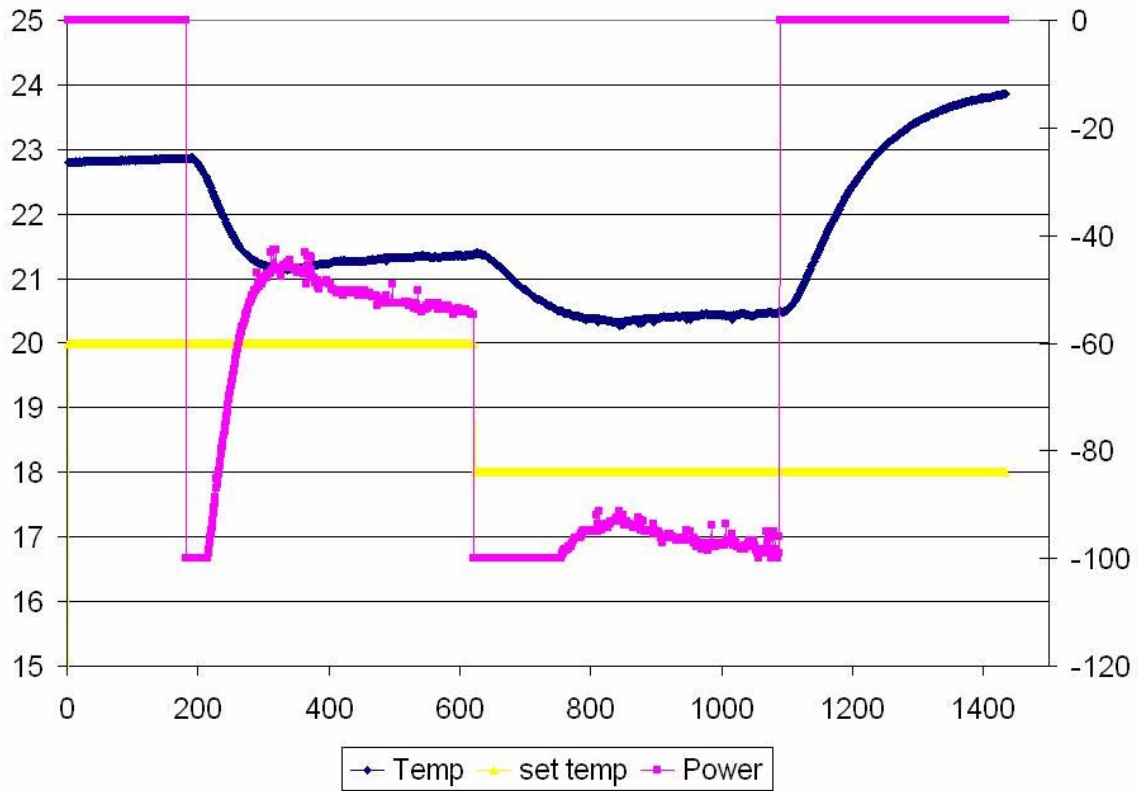


Figure 20. Test of temperature control system with two set points.

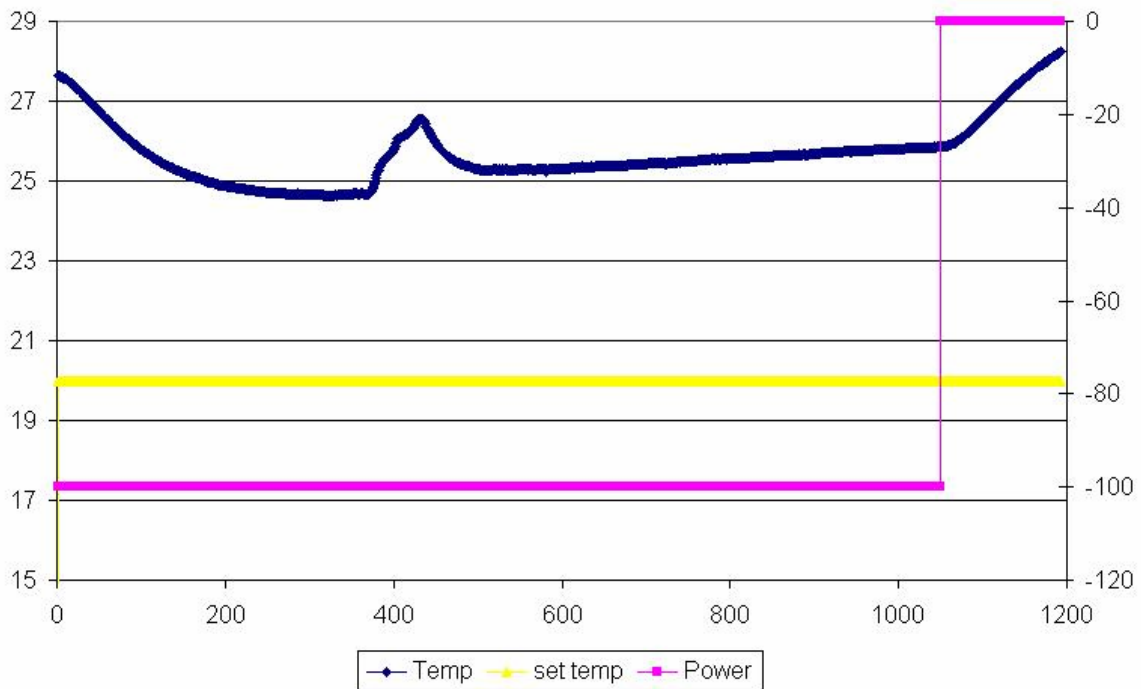


Figure 21. Test of temperature control system in which the chamber was opened and the inner heat sink temperature examined.

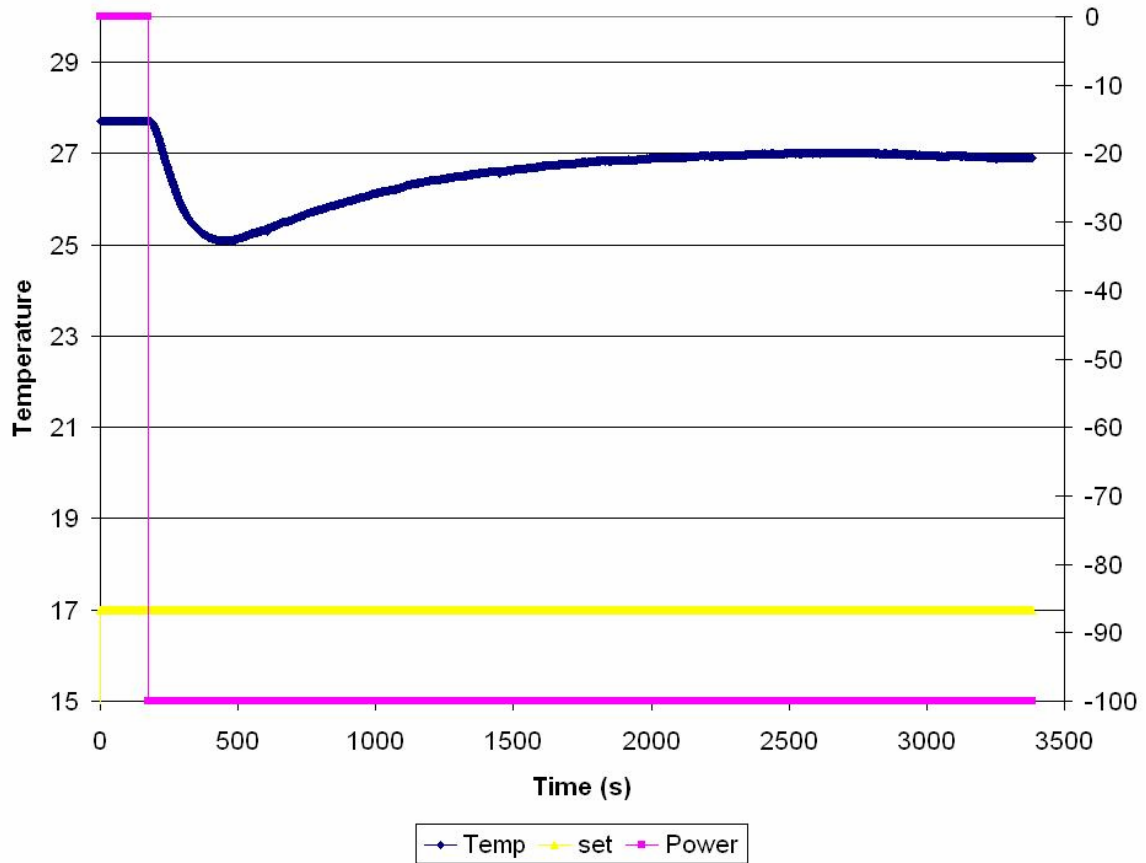


Figure 22. Test of temperature control system in which the controller RTD was attached to the heat sink rather than laying in front of it. The chamber was also fitted with thermocouples as in the mixing test.

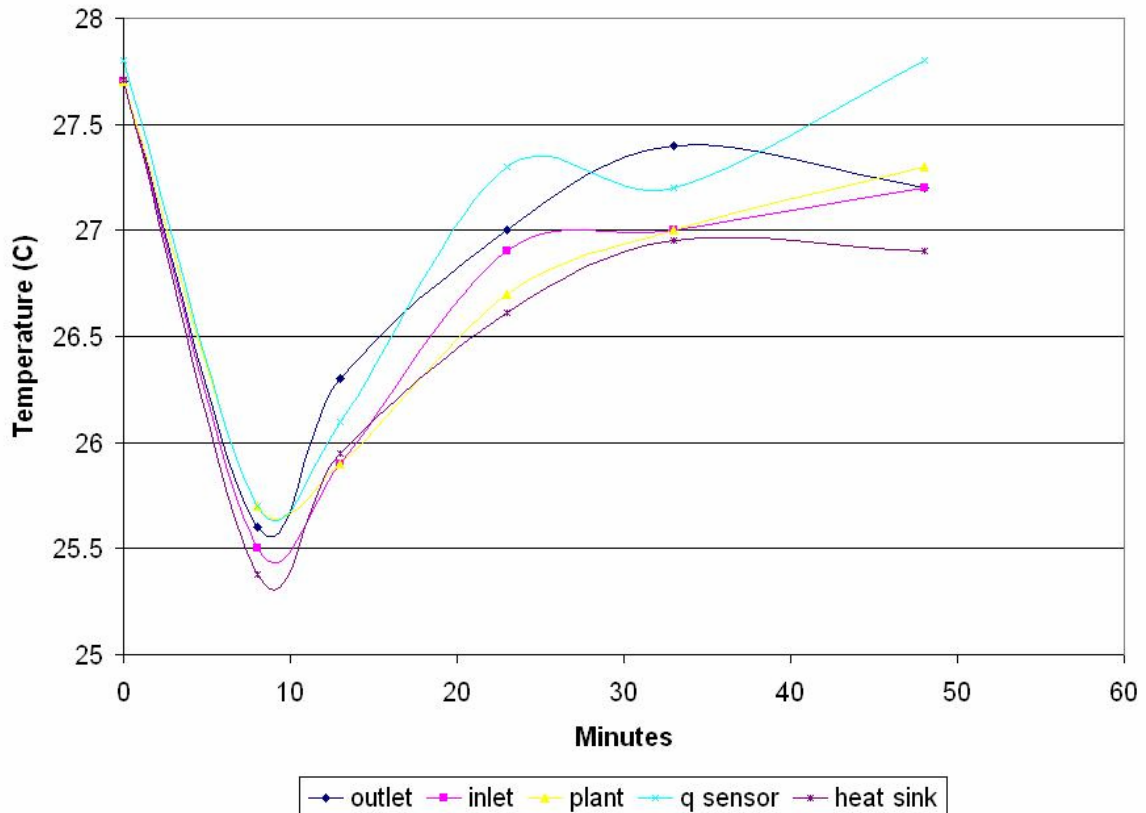


Figure 23. Test of temperature control unit with data from same test as directly above. The temperature in the rest of the chamber generally followed the temperature at the heat sink, indicating acceptable movement of heat between the chamber and the inner heat sink.

### Humidity Control Column Tests

#### On dehumidifier column: RH

Ambient	Post-Dehumidifier
33.60%	5.50%

#### On humidifier column: RH

Ambient	Post-humidifier
31.50%	102.80%

#### On null column: RH

Ambient	Post-null
35.10%	34.80%

Table 2. Initial humidity column test results. This test was operated an initial test at a lower flow rate than design.